Fabian Niess

MR Pulse Sequence Development for Localized Dynamic Spectroscopy with 7T

Master's Thesis

Graz University of Technology

Institute of Medical Imaging
Head: Univ.-Prof. Dipl.-Ing. Dr.techn Rudolf Stollberger
Supervisor: Univ.-Prof. Dipl.-Ing. Dr.techn Rudolf Stollberger

Conducted at Medical University of Vienna under the Supervision of:
Assoc.-Prof. Dr. Martin Meyerspeer

Graz, April 2015

This document is set in Palatino, compiled with pdfLaTeX2e and Biber.

The LaTeX template from Karl Voit is based on KOMA script and can be found online: https://github.com/novoid/LaTeX-KOMA-template

Statutory Declaration

I declare that I have authored this thesis independently, that I have not used other than the declared sources/resources, and that I have explicitly marked all material which has been quoted either literally or by content from the used sources.

Graz, _____ _____

Date Signature

Eidesstattliche Erklärung[1]

Ich erkläre an Eides statt, dass ich die vorliegende Arbeit selbstständig verfasst, andere als die angegebenen Quellen/Hilfsmittel nicht benutzt, und die den benutzten Quellen wörtlich und inhaltlich entnommenen Stellen als solche kenntlich gemacht habe.

Graz, am _____ _____

Datum Unterschrift

[1] Beschluss der Curricula-Kommission für Bachelor-, Master- und Diplomstudien vom 10.11.2008; Genehmigung des Senates am 1.12.2008

Abstract

^{31}P spectroscopy using a semi-LASER sequence (Localization by Adiabatic Selective Refocusing) at 7 T allows dynamic analysis of metabolism in exercising human muscles with a high time resolution e.g. ($T_R = 6$ s), good specificity and a satisfying signal to noise ratio even in small volumes. To investigate the effect of exercise to different muscles groups with a single voxel spectroscopy technique, separate measurements have to be acquired. This means that the subject has to repeat the exercise for every acquired volume of interest (VOI), which is time consuming and potentially inflicts a physiologic influence of the preceding exercise on the second measurement.

In this thesis the idea of multiple voxel acquisition is picked up and implemented with the semi-LASER acquisition scheme using the pulse programming environment of Siemens, to allow an interleaved measurement of two independent volumes within one repetition.

The user interface was modified to enable the selection of multiple independent VOIs, and phantom measurements were performed on the 7 T Siemens MAGNETOM scanner at the Center for Medical Physics and Biomedical Engineering at Medical University Vienna. To evaluate the performance and to illustrate mutual influences between the volumes during multi volume acquisition, results of both single and multi voxel spectroscopy measurements were compared. Furthermore in vivo measurements were performed to practically test the functionality and usability of the sequence. It offers the opportunity to acquire more information within the same time, i.e. from different regions, and therefore can help to improve the interpretation of dynamic MRS data in metabolic research.

Contents

List of Figures

1 Introduction

Spectroscopy in general describes the interaction between electromagnetic radiation and matter based on the principles of the atomic or molecular absorption and emission. Dependent on the field of application, spectroscopy is used to identify and analyze certain metabolic concentrations in a compound in vitro and in vivo. With most spectroscopic methods the interaction between the outer electrons of matter and the incoming electromagnetic radiation requires very small wavelengths in the ultraviolet range [1].

This thesis focuses on the field of Nuclear Magnetic Resonance Spectroscopy ^{31}P NMR spectroscopy in particular. In contrast to the methods mentioned above, NMR uses longer wavelengths in the RF range to excite the metabolites. NMR is the study of absorption and emission of electromagnetic radiation from different nuclei in presence of a strong magnetic field [1].

1.1 History

NMR was first discovered in 1946 by two independent groups of physicists: Purcell, Torrey and Pound [2] at MIT, Cambridge and Bloch, Hansen and Packard [3] in Stanford, concurrently. In 1952 Bloch and Purcell both shared the Nobel Prize [1].

In the beginning NMR was used by physicists and chemists as an experimental method, to investigate nuclear moments of different nuclei. The discovery that energy is absorbed at different frequencies in the same molecule what is now known as chemical shift was the breakthrough of the modern NMR spectroscopy [1]. The chemical shift was first described in 1950 by Proctor and Yu [4] and simultaneously by Dickinson[5].

In the first 20 years the signal was acquired in the continuous wave-mode, changing the frequency of the RF wave and passing through the spectral range of interest, while the other magnetic field is static.[1]

Ernst and Anderson [6] first came up with the pulsed NMR in combination with the Fourier transformation of the acquired signal, which revolutionized the application of NMR spectroscopy. The spin excitation with RF pulses is not harmful to human tissue and noninvasive. Therefore it is ideal for in vivo applications even though NMR spectroscopy is rather insensitive due to the low photon absorption compared to other spectroscopy techniques. [1]

It was shown by Moon and Richards that it is possible to determine the pH in the red blood cells with ^{31}P MRS [7].

1.2 Application

Nuclear magnetic resonance spectroscopy is common method to analyze different metabolic compounds in vitro and in vivo. For studying the metabolic response in muscle tissue during exercise ^{31}P MRS is often used, which allows analyzing high energy phosphates in small quantities [8].

With clinical standard field strengths (0.5 T-3 T) ^{31}P MRS has to deal with low signal to noise ratio compared to proton MRS. With unlocalized ^{31}P MRS the voxel of interest (VOI) is only defined by the coil sensitivity profile instead of gradient based localization methods where only a desired volume is excited and measured [1]. The increase of specificity when using localization comes at the price of lower sensitivity and signal to noise ratio and as a compensation, multiple signal averaging would be necessary, which directly affects temporal resolution [9]. With the introduction of ultra-high field (7 T)MR scanner, dynamic localized ^{31}P MRS with an acceptable signal to noise ratio and a high temporal resolution was possible as mentioned in the work of Meyerspeer et.al. where ^{31}P MRS spectra were acquired with a semi-LASER sequence (Localization by Adiabatic Selective Refocusing) and compared to unlocalized spectra [8], [9].

When it comes to analyzing specific muscles with ^{31}P MRS it is obvious to talk about measuring two spectra of different muscles interleaving during one acquisition. Ernst and Henning presented a method to acquire two ^{1}H NMR spectra of two different voxel in an interlaced mode using a PRESS sequence [10]. They showed that with tilted gradients the two voxels do not share the same slices during excitation and refocusing, so the RF pulses do not cause mutual saturation [10]. The measurements were applied with local shimming of each voxel individually with an echo time of 135 ms from 2 mm^2 voxels and a T_R=1700 ms with 256 averages [10].

This thesis focuses on developing the already available semi-LASER sequence which is described in 3.3 in more detail, for dynamic localized ^{31}P MRS in a human calf muscle [8], [9], [11] to a multi voxel spectroscopy sequence via IDEA provided by SIEMENS to measure two voxels interleaving during one repetition, and show the mutual saturation effects on both voxel if they share the same slices during RF excitation and refocusing pulses.

2 Basic NMR Principles

The content of the following chapter mainly orientates on Robin A. de Graafs book "In Vivo NMR Spectroscopy" [1] and the script of Rudolf Stollberger [12]. The nuclear magnetic resonance is based on the presence of a nuclear spin. Therefore the atomic nuclei interacts with different other particles for example other nuclei, the outer electrons of the same atom and the electrons of the whole molecule [12].

2.1 The Approach of Classical Physics

To describe an effect at the atomic level, a quantum mechanical approach is necessary but in case of NMR the classical physics approach is also useful. In classical physics an object with a mass m rotating constantly about a fixed point with the radius r, has an angular momentum L which can be defined in respect to Newtons first and second law as:

$$\vec{L} = m(\vec{r} \times \vec{v}) \tag{2.1}$$

It is also known that if an object is charged and moves along a closed path, a current loop is created and therefore the object has a magnetic moment μ, which in general is defined as current times area. In case of a nuclei with charge e and velocity v the magnetic moment is defined by:

$$\mu = \left[\frac{ev}{2\pi r}\right] \pi r^2 \tag{2.2}$$

(2.1) and (2.2) combined reveales the important relation between the angular and the magnetic moment where γ is the gyromagnetic ratio:

$$\vec{\mu} = \left[\frac{e\vec{v}}{2\pi\vec{r}}\right]\pi\vec{r}^2 = \left[\frac{e\vec{v}}{2}\right]\vec{r} = \left[\frac{e}{2m}\right]m(\vec{r}\times\vec{v}) = \left[\frac{e}{2m}\right]\vec{L} = \gamma\vec{L} \tag{2.3}$$

The gyromagnetic ratio is different for each nucleus. When an object with a magnetic moment is placed in a magnetic field $\vec{B_0}$ it will perceive a torque $\vec{T}$

$$\vec{T} = \vec{\mu}\times\vec{B_0} \tag{2.4}$$

With the knowledge that an angular moment only can be changed with an applied torque, (2.3) and (2.4) this can be combined into:

$$\left(\frac{d\vec{\mu}}{dt}\right) = \gamma\vec{\mu}\times\vec{B_0} \tag{2.5}$$

Finally it is known that the orientation of $\vec{\mu}$ depends on $\vec{B_0}$ so the precession of $\vec{\mu}$ about $\vec{B_0}$ can be written as:

$$\left(\frac{d\vec{\mu}}{dt}\right) = \vec{\mu}\times\vec{\omega_0} \tag{2.6}$$

Combining (2.5) and (2.6) the final larmor equation is derived[1]:

$$\vec{\omega_0} = \gamma\vec{B_0} \tag{2.7}$$

$$f = \left(\frac{\gamma}{2\pi}\right)B_0 \tag{2.8}$$

2.2 Quantum Mechanical Approach

This approach includes the fact that spins can only have certain discrete values depending on the spin quantum number I, which further depends on the atomic mass number. The angular momentum L and the angular moment in z-direction L_z is also limited to discrete values as shown in (2.9) and (2.10).[1], [12]

$$L = \hbar\sqrt{I(I+1)} \tag{2.9}$$

$$L_z = \hbar m_q \tag{2.10}$$

To not confuse the second quantum number with the mass m it is written as m_q.

$$m_q = I, I-1, I-2, ..., -I \tag{2.11}$$

In the case of protons, a particle with spin quantum number I = $\frac{1}{2}$ the second quantum number m_q can only have the values $-\frac{1}{2}$ and $\frac{1}{2}$. (2.3) is also valid for the quantum mechanical approach and combined with (2.10) the magnetic moment in z-direction is [1]:

$$\mu_z = \gamma\hbar m_q \tag{2.12}$$

The energy difference between the state of the magnetic moment parallel and antiparallel in the magnetic field can be summarized to:

$$\triangle E = -\triangle \mu B \tag{2.13}$$

Einsteins equation for electromagnetic radiation with the Plancks constant h and the frequency f can be combined with (2.12) and (2.13) and the same result as with the classical approach is derived.

$$E = hf = \hbar\omega \tag{2.14}$$

$$f = \left(\frac{\gamma}{2\pi}\right) B_0 \tag{2.15}$$

2.3 Magnetization

The macroscopic magnetization vector M_0 is the representative of the sum of all magnetic moments. There is no net component in the xy-plane because the spins are randomly distributed around the z-axis. Figure 2.1 shows the case of protons or any other $\frac{1}{2}$ spin nucleus, where the two different energy states parallel (low energy) and antiparallel (high energy) are almost evenly distributed with a significant small population difference in favor for the parallel spins. The fraction of spins which are aligned parallel is about 3 ppm higher than the antiparallel majority.[1], [12]

With the Boltzmann statistic it is possible to determine this distribution given by:

$$\left(\frac{n_\alpha}{n_\beta}\right) = \mathrm{e}^{\triangle E/kT} \tag{2.16}$$

Where n_α is the number of spins parallel and n_β is the number of spins antiparallel with the Boltzmann constant k and the temperature T. Figure 2.2 shows the relation between the energy difference of the two states of alignment and the external magnetic field strength. At body temperature (37°C) the thermal energy is obviously higher than the energy difference, and the equation can be simplified to:

$$\left(\frac{n_\alpha}{n_\beta}\right) = 1 + \left(\frac{h\upsilon}{kT}\right) \tag{2.17}$$

At thermal equilibrium the magnentisation vector M_0 is:

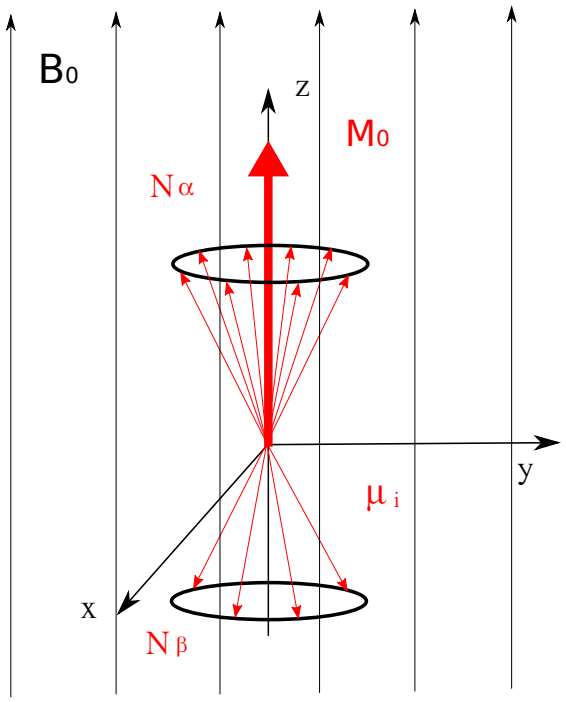

Figure 2.1: Macroscopic spin distribution according to the Boltzmann statistics with two possible orientations. Figure reproduced from [12]

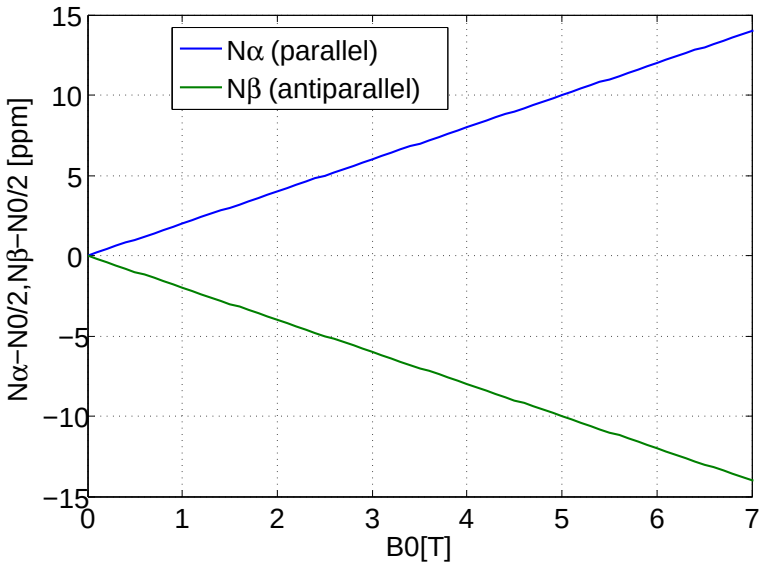

Figure 2.2: The spin energy of a proton as a function of the external applied magnetic field B_0. Figure reproduced from [12]

$$M_0 = \sum_{i=1}^{n} \mu_i = n_\alpha \mu_z + n_\beta \mu_z = \gamma \left(\frac{h}{4\pi} \right) (n_\alpha - n_\beta) \tag{2.18}$$

With the assumption that $(h\nu/kT) << 1$ and $n = n_\alpha + n_\beta$ where n is the total number of spins and (2.17) the population difference is given by:

$$(n_\alpha - n_\beta) \approx \left(\frac{nh\nu}{2kT} \right) \tag{2.19}$$

The magnetization $\vec{M}_0$ is therefore at thermal equilibrium:

$$\vec{M}_0 = \left(\frac{\gamma h}{2\pi} \right)^2 \left(\frac{n\vec{B}_0}{4kT} \right) \tag{2.20}$$

Now it is clear that the only variable parameter for applications in vivo is the magnetic field strength B_0 because the temperature is constant [12].

2.4 Chemical Shift

The gyromagnetic ratio (2.7) shows, that the Larmor frequency depends on both the type of nuclei and the external magnetic field strength B_0. Another influence which changes the Larmor frequency locally is the chemical environment of each nucleus and this is called Chemical Shift.

The electrons surrounding the nuclei are carrying an electric charge and causing a magnetic moment μ_e as shown in (2.2). The electrons are precessing in the opposite sense to the nuclear precession and therefore reduce the magnetic field sensed by the nuclei as shown in Figure 2.3 If the local magnetic field varies, it changes also the local Larmor frequency.

By exploitation of this phenomenon it is possible to determine different metabolic concentrations in a sample based on the chemical bonds of the

nuclei. Otherwise a sample containing one type of nuclei would only resonate at one frequency and NMR spectroscopy would be far away of todays importance[1].

The shielding can be written as:

$$B = B_0(1 - \sigma) \tag{2.21}$$

where σ is a dimensionless constant which represents the shielding and depends on the chemical environment.

In combination with (2.7) the Larmor equation can be written as:

$$f = \left(\frac{\gamma}{2\pi}\right) B_0(1 - \sigma) \tag{2.22}$$

Chemical shifts are expressed in parts per million [ppm] so it is easier to compare them between different magnetic field strengths B_0. The Chemical Shift is defined as:

$$\delta = \frac{f - f_{ref}}{f_{ref}} \times 10^6 \tag{2.23}$$

In NMR spectroscopy it is always necessary to have a reference (2.23). It is possible to use either an external or an internal reference. For in vivo systems it is common to use internal references. For brain ^{1}H MRS the internal reference is N-acetyl aspartate (2,01 ppm) and for ^{31}P MRS it is phosphocreatine (0,00 ppm).[1]

2.5 Radiofrequency Pulses

In magnetic resonance imaging and magnetic resonance spectroscopy of course it is necessary to acquire a processable signal (free induction decay) from the investigated sample. The spins which are aligned with an applied external magnetic field B_0 in z direction have to be deflected into the

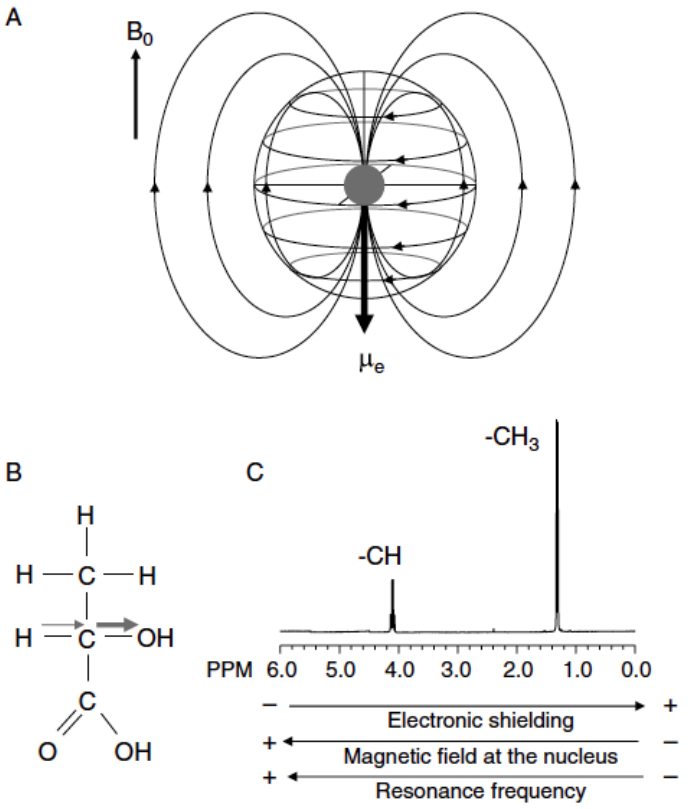

Figure 2.3: (A) The electrons with the electric charge e are causing the magnetic moment μ_e which counteract the external magnetic field and so the effective magnetic field sensed by the nucleus is reduced. (B) The oxygen atom is more electronegative than the hydrogen and so it shifts the electrons away from the hydrogen which inhibits the shielding and increases the local Larmor frequency. (C) In this NMR spectrum the methine proton is closer to the oxygen than the three methyl protons and has therefore a higher Larmor frequency. Figure reproduced from [1]

transversal xy plane. After the excitation the spins relaxate back in the initial state and generate a detectable signal in the receiver coil due to induction. Only the transversal components yield a signal. [1].

Radiofrequency pulses are used to perform such a spin manipulation in a given frequency range for instance: excitation, inversion or refocussing. The frequency of the RF pulse has to equal the Larmor frequency of the sample to allow energy transfer with the spins.[12] Therefore it is possible to selectively excite a particular slice of interest by applying a gradient field across the probe along one specific direction during the RF-Pulse, which overlaps with the B_0 field and constantly change the local Larmor frequency according to the spatial position. In combination with an applied RF pulse with a corresponding frequency bandwitdh according to the desired slice thickness, only the spins in that slice will align in the xy plane. [1]

There are several types of pulse-shapes for example a nonselective square pulses or ”hard” pulses which excite a broad frequency bandwidth with a constant amplitude and a short duration as the Fourier transformation of a rectangle function is a Sinc function. Hard pulses are used if a short duration is required for example in a combination of hard pulses also known as composite pulses. [13] The general behavior of composite pulses is the same as a single hard pulse but with greater insensitivity to B_1 inhomogeneities. [1]. More commonly used are frequency-selective pulses with a Sinc or Gauss function in the time domain which is a rectangle or a Gauss function in the frequency domain. [1] Increasingly popular are RF pulses which follow adiabatic principles as they are amplitude and frequency modulated and consist of hundreds of hard pulses similar to composite pulses with varying amplitude and phase. Adiabatic pulses are longer in duration but are insensitive to B_1 inhomogeneities. [1]

In this master thesis a semi-LASER sequence was used with adiabatic refocussing pulses and a slice selective Sinc-shaped excitation pulse.

2.6 Adiabatic Pulses

For RF pulses with constant amplitude and constant carrier frequency ω_c the nutation angle θ depends linearly on the B_1 amplitude:

$$\theta = \gamma B_1 T \tag{2.24}$$

If the B_1 field is spatially inhomogeneous it will lead to signal loss and artifacts because a variety of nutation angles will be generated over the volume. [14]

For in vivo measurements high sensitivity in signal reception is required and therefore surface coils are often used. The main disadvantage is the highly inhomogeneous B_1 field generated by the coil and this causes signal loss and artifacts if classical RF pulses are applied. To solve this problem it is possible to excite the spins with a volume coil and receive the signal with a surface coil but it is difficult to arrange the coils orthogonal to prevent inductive coupling which would lead to signal loss.[1]

In this case it is more convenient to use adiabatic RF pulses. Adiabatic pulses are more insensitive to B_1 inhomogeneities than composite pulses and generate a uniform nutation angle even with smaller B_1 amplitudes. [1]

With adiabatic pulses the carrier frequency varies with time while applying the pulse and sweep through the frequency range of interest. If the pulse duration is short relative to the T_1 time, the pulse can be used the same way as conventional pulses. [14]

Across the bandwidth the spins with different precession frequencies rotate as the frequency of the pulse approach their Larmor frequency. The range of the frequency sweep only defines the bandwidth. With conventional pulses the pulse duration T_p is always inverse proportional to the bandwidth $\triangle\Omega$ but in case of adiabatic pulses the bandwidth and the pulse duration are independent parameters. This allows to rotate spins across a wide bandwidth with a relatively low B_1 amplitude. [14]

2.6.1 Visualization

In a reference frame $(x'y'z')$ that rotates with ω_{RF}, the direction of the B_1 vector is static during the application of an adiabatic RF pulse. If the frequency of the pulse differs from the Larmor frequency of the observed spin, it generates a magnetic field along the z'-axes with an amplitude equal to $\triangle\omega/\gamma$ where $\triangle\omega = \omega_0 - \omega_{RF}$. The effective field B_{eff} is the vector sum of $\triangle\omega/\gamma$ and B_1. During an adiabatic passage the frequency constantly changes and therefore the effective field vector changes its direction at the angular velocity $d\alpha/dt$ along the x' - axis where [14]:

$$\alpha(t) = \arctan\left[\frac{\gamma B_1(t)}{\triangle\omega(t)}\right] \tag{2.25}$$

At the beginning of the pulse where $\omega_{RF} << \omega_0$, $\triangle\omega/\gamma$ is very large relative to B_1 and therefore the effective field direction is almost parallel to the z-axis. While ω_{RF} approaches ω_0, $\triangle\omega(t)$ decreases and finally vanishes so B_1 equals B_{eff}. At this point an Adiabatic Half Passage is completed. For an Adiabatic Full Passage the frequency has to decrease to $-\triangle\omega_{max}$. As shown in Figure 2.4:

During the adiabatic pulse the Magnetization Vector M follows B_{eff}. The Visualization in the Frequency modulated (FM) frame is not descriptive, so for for the adiabatic passage a B_{eff}-frame $(x''y''z'')$ is used where the frame rotates with $d\alpha/dt$ around the y' axes. At the beginning the two frames are congruent. As the frequency sweeps across the bandwidth the B_{eff}-frame starts to rotate. The B_{eff}-vector always stays collinear with the z''-axes. [14]

This rotation around the y′-axes generates a magnetic field with the magnitude $d\alpha/dt/\gamma$ in y′-direction as shown in Figure 2.5b. The vector sum of B_{eff} and this magnetic field is the resultant magnetic Vector E(t). The magnetization M precesses around E with the angle ϵ and if the adiabatic condition is satisfied ϵ is very small and it is assumed $B_{eff} = E(t)$. This means that for components of M which are perpendicular to B_{eff} at the beginning of the pulse, the angle between M and B_{eff} varies between $90 \pm \epsilon$ but stays almost perpendicular during the whole pulse. The same applies to components which are initially parallel to B_{eff}. [14]

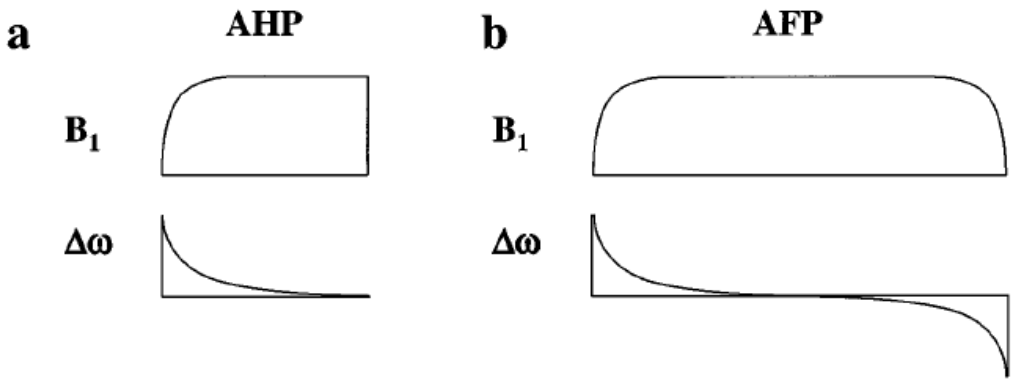

Figure 2.4: Examples of two types of pulses of the adiabatic passages: (a) adiabatic half passage and (b) adiabatic full passage. Figure reproduced from [14]

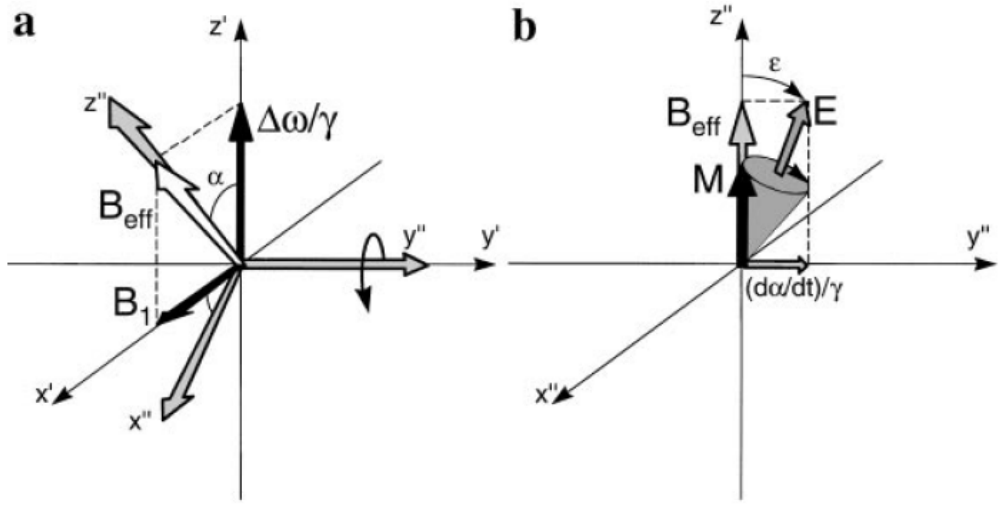

Figure 2.5: Vector diagrams of the two rotating frames to describe an adiabatic passage. (a) Correlation between the frequency modulated frame (FM) and the B_{eff} frame b. Figure reproduced from [14]

3 NMR Spectroscopy

With NMR spectroscopy it is possible to determine different metabolic compound concentrations in a probe or in vivo according to their chemical shift as mentioned earlier in section 2.4. It is possible to excite different nuclei by applying RF pulses with the corresponding Larmor frequency for example ^{1}H , ^{31}P , ^{13}C , ^{23}Na , ^{39}K or ^{19}F. This thesis focuses on ^{1}H MRS and especially ^{31}P MRS with single voxel spectroscopy in more detail [1].

The excitation is followed by refocusing of the magnetization after $T_E/2$ in case of a spin echo sequence which generates an echo at T_E. The minimum echo time T_E is composed of the sum of the excitation and refocusing pulse duration and eventual spoiler gradient duration.

Due to induction the echo signal is obtained in a receiver coil and a following Fourier tranformation results in the desired spectrum [1]. During excitation it is possible to yield the signal of the whole volume (unlocalized) or to apply localization techniques to acquire only the signal of a specific volume of interest which is described in more detail in section 3.1.

Beside the fact that hydrogen nuclei yield the most signal magnitude compared to other biologic relevant nuclei e.g ^{31}P because of its high natural abundance, there are some influences which make ^{1}H MRS quite challenging [1]. When it comes to ^{1}H MRS the water signal magnitude is significantly higher than most of the metabolites of interest and therefore the water resonance has to be suppressed by preliminary RF pulses [1]. Furthermore unlocalized ^{1}H MRS of the brain can suffer contamination by extracranial lipids, resulting in an interference with the small metabolites of interest. This can be eliminated when applying localization techniques which use gradient based volume selection. These gradients can also cause a lipid contamination because of possible chemical shift displacements artifacts which are later described in section 3.1.2. Additionally B_0 inhomogeneities

highly affects spectral resolution. All these effects demand localization and water suppression techniques to achieve meaningful spectra [1]. Another limitation of ^{1}H MRS is the small chemical shift range of the metabolites with about 5 ppm resulting in an overlap of the resonances [1].

The application of ^{31}P MRS is not affected by the influences of water signal and lipid contamination except possible B_0 field inhomogeneities, but the sensitivity is significantly lower with about 7 % of protons [1]. With a wide chemical shift range of about 30 ppm it is possible to acquire spectra with a good spectral resolution even at lower field strengths (0.5 T-1.5 T) but this will be discussed later in 3.2.

3.1 Localization in Magnetic Resonance Spectroscopy

After transmission of an excitation pulse and without any additional effort the receiver coil receives the signal sum of the whole volume consisting of the desired nuclei bound differently in individual molecules. The volume of interest (VOI) is only defined by the sensitivity profile of the coil and this is known as unlocalized NMR spectroscopy [9].

Localization in NMR spectroscopy is used to receive a signal from a defined region of interest (ROI) only either by selective excitation of the desired region or by suppression of the surroundings. Localization minimizes artifacts when the surrounding tissue yield a signal which influences the VOI (partial volume effect) and the inhomogeneities of B_0 and B_1 are very small over a small voxel compared to unlocalized signal detection. The detected spectral lines are narrower and it allows a uniform excitation and reception as can be seen in Figure 3.1[1]. Beside the benefits, localization comes at the cost of lower signal to noise ratio per unit time and leads to averaging the signal to increase SNR. The SNR increases with the number of averages N as shown in (3.1) [9]

$$SNR \propto \sqrt{N} \tag{3.1}$$

As shown in figure Figure 3.1 the unlocalized spectra of ^{1}H MRS of a piglet brain is highly influenced by extracranial lipids and would not allow a differentiation of the metabolites. This is not the case when it comes to ^{31}P MRS.

3.1.1 Single Voxel Localization

In general localization principles are used with an applied gradient field in one specific direction, which changes the local B_0 field according to the spatial position. B_0 changes directly affect the local Larmor frequency according to (2.7) and therefore the local frequency depends also on the spatial position.The slice thickness is defined with the bandwidth of the applied RF pulse. This is repeated for all three orthogonal directions to define the 3D voxel of interest. There are two basic principles to apply localization: outer volume suppression (OVS) and single voxel spectroscopy (SVS). OVS manipulates the magnetization to inhibit unwanted signals from outside. This thesis focuses on single voxel spectroscopy applied as a semiLASER sequence which is described later in 3.3. Single voxel localization specifically excites only the spins in the volume of interest. In case of SVS a slice selection gradients are switched on and off during the excitation and refocusing pulses as mentioned before. [1].

3.1.2 Chemical Shift Displacement Artifacts

During localization a linear dependence between the chemical shift of the sample under investigation and the spatial position is observed. In the presence of a field gradient G_x the Larmor frequency of the spins changes linearly with the position in x-direction as shown in equation (3.2) and (3.3) [1]:

$$\omega(x) = \omega_0 + \gamma G_x \tag{3.2}$$

$$x = \frac{\omega(x) - \omega_0}{\gamma G_x} \tag{3.3}$$

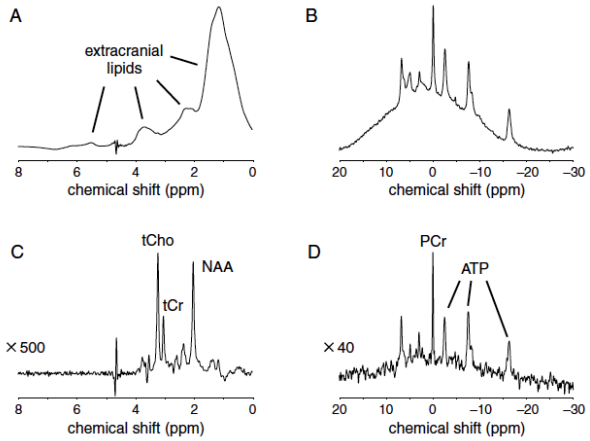

Figure 3.1: Comparison of unlocalized and localized NMR spectra (A) Unlocalized ^{1}H MRS and (B) ^{31}P MRS spectra. (C) Localization applied with PRESS and it is now possible to determine the different compounds (D) Localization is done with ISIS. The difference between unlocalized and localized in ^{31}P MRS is not that significant compared to ^{1}H MRS [1]

Additionally there is a difference in Larmor frequency between two different compounds and therefore a spatial displacement is observed from one type of nuclei relative to the other as shown in equation (3.4) and Figure 3.2 where $\triangle\omega$ represents the difference in Larmor frequency [1]:

$$\triangle x = \frac{\triangle\omega}{\gamma G_x} \tag{3.4}$$

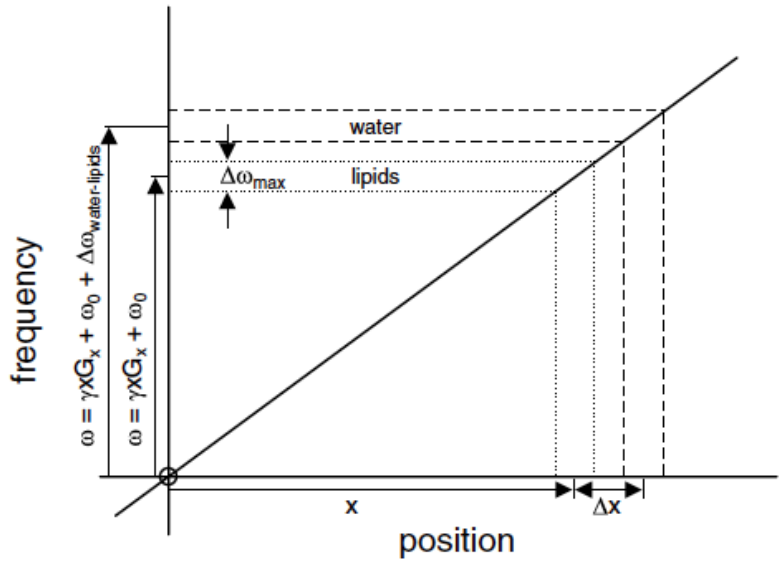

Figure 3.2: The Larmor Frequency as a function of the spatial position x. If a RF pulse is applied at a frequency $\omega_0 + \gamma x G_x$ while a field gradient G_x is switched on to select a slice at position x the frequency difference between water and lipids leads to a displacement and a selected slice at $x + \triangle x$ [1]

It is very important to select a suitable resonance reference to avoid such chemical displacement artifacts especially in ^{1}H MRS and ^{1}H MRI where the frequency shift between water and lipids is about 3.5 ppm. Acquiring the signal relative to the water resonance results in shifting the slice selection for fat, according to (3.4). This can cause lipid contamination if the voxel is placed close to fat tissue [1]. Choosing a reference close to lipid frequency e.g NAA could prevent contamination.

As the chemical shift displacement increases with higher magnetic field strength it is possible to increase gradient strength and simultaneously increase the bandwidth of the RF pulse to maintain the same voxel dimensions but this leads to a shorter RF pulse duration which increases the specific absorption rate or reach the pulse voltage limits of the coil. [1], [8].

Contaminations can be minimized when using localization and prevent chemical shift displacement artifacts but imperfections of the RF pulse frequency profile could also lead to such artifacts. As shown in Figure 3.3 during localization, the real slice profile of the RF pulse slightly differs from the ideal rectangular pulse which could cause contaminations outside the selected slice [1].

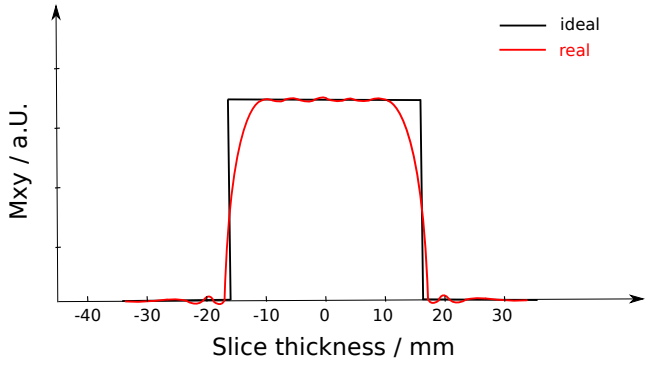

Figure 3.3: Slice Profile of an ideal and a real RF pulse during localization when the slice selective gradient is switched on.

3.1.3 Eddy Currents

The fast switching of local field gradients has of course its side effects because according to Farradays law every time-varying magnetic field will induce a current in a close conductor and therefore also a time varying magnetic field is generated, which counteracts with the first. The so-called eddy currents can cause a distortion of the desired waveform of the gradient and this leads to artifacts in magnet resonance imaging and distortions in magnetic resonance spectroscopy [1].

There are some techniques available to compensate eddy currents for instance pre-emphasis where complex electric circuits generate a specific waveform of a gradient field which in a superposition with the eddy current induced gradient field results in the desired waveform of the gradient as shown in Figure 3.4 [1].

The second approach to decrease eddy currents is active shielding, where the magnetic field lines outside the active volume will be reduced via specifically positioned wires on the outside of the coil with an opposite current. As shown in Figure 3.5 the magnetic field lines can expand far outside the coil and can induce currents in nearby conductors. Placing several wires outside the loop can reduce the magnetic field lines outside the active volume significantly [1].

In most MR systems a combination of both techniques is combined to reduce eddy currents [1].

3.1.4 Ultra High Field

In case of ^{31}P MRS when the muscle metabolism is under investigation and a dynamic measurement is applied, temporal resolution is an important factor and therefore averaging highly affects the performance. Especially when working at lower field strength (1.5 and 3 T) dynamic localized ^{31}P MRS spectroscopy reaches the limits because of the longer T_1 relaxation and the lower SNR. These drawbacks are reduced when working at a ultra high field scanner (7 T) [9].

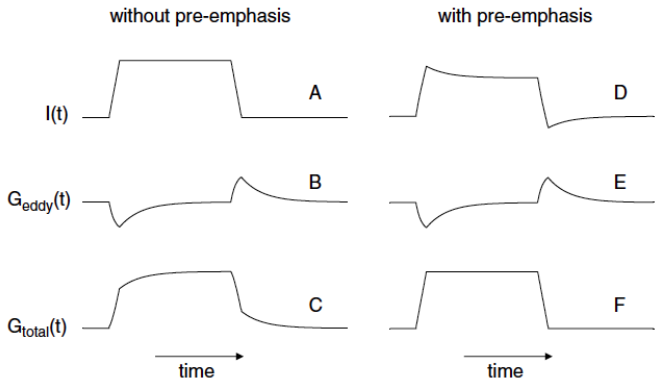

Figure 3.4: Pre-emphasis. According to Faradays law a fast switched current induces a time varying gradient field which induces so-called eddy currents in nearby conducting materials which further induces a second time varying gradient field which counteracts the first. (C) is the superposition of the desired gradient in the waveform of (A) and the eddy current generated gradient field (B). With pre-emphasis a specific waveform is selected that the induced gradient field of (D) in combination with the eddy current generated field (E) results in the desired waveform (F). Figure reproduced from [1]

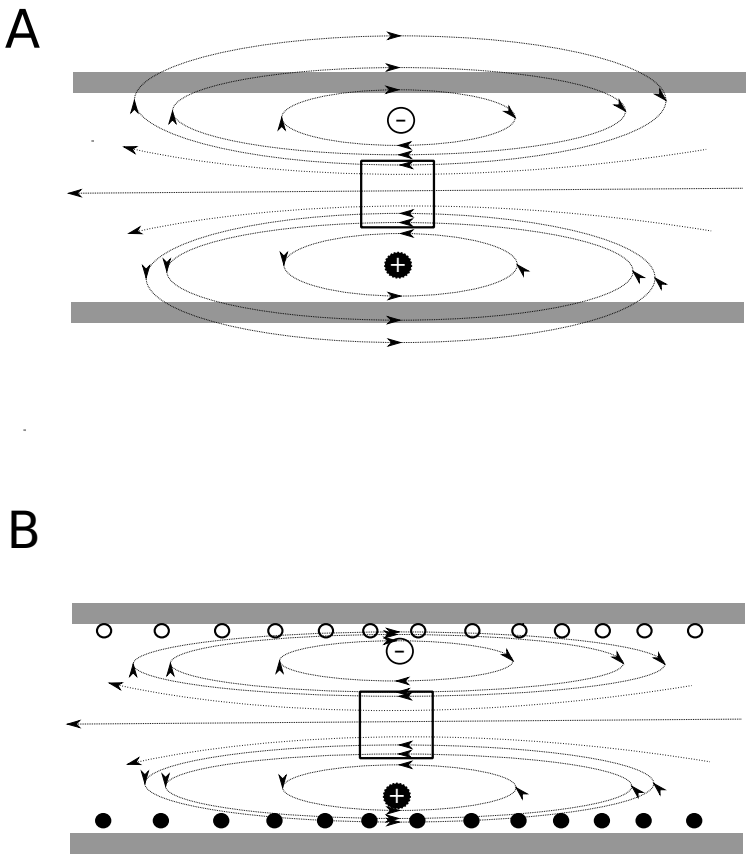

Figure 3.5: Active shielding shown with a single loop. (A) shows the magnetic field lines occur outside of the active volume and can induce currents in nearby conducting materials. Placing a few wires outside the coil carreying current with the opposite direction as the coil, it reduces the magnetic field lines outside the volume. Figure reproduced from [1]

Increasing the magnetic field strength also has a big impact when it comes to susceptibility artifacts, which depend linearly on the field strength and this counteracts the SNR gain. Also the spectral dispersion increases which requires a bigger RF bandwidth and therefore shorter RF pulses. Shortening the pulses is limited by reaching the specific absorption rate limits [1], [8].

3.2 Phosphorus Spectroscopy

Magnetic resonance spectroscopy in general and phosphorus spectroscopy in particular is commonly used to analyze energy metabolism in muscle tissue. ^{31}P MRS measures concentrations of phosphates in absolute or relative quantities. [8][1]. With phosphorus spectroscopy it is possible to acquire signals with a high spectral resolution even at low magnetic field strengths (B_0) due to the large chemical shift dispersions between the phosphate compounds in vivo, which are about 30 ppm. Additional it is possible to derive biologic parameters e.g. intracellular pH [1].

3.2.1 Resonance Frequencies

There are only a few ^{31}P-containing metabolites which are biologically relevant, which can be found in table3.1 with their corresponding chemical shift dispersions. [1]

The individual resonances of each compound are sensitive to pH changes and ionic concentrations. Typically phosphocreatine (PCr) is used as an internal reference at 0.00 ppm. Typical resonances in vivo at a pH 7.2 are for inorganic phosphate 5.02 ppm and for ATP $-7.52(\alpha)$, $-16.26(\beta)$,$-2.48(\gamma)$ [1].

Figure 3.6 shows spectra of different tissues in a rat with localized ^{31}P MRS.

Table 3.1: Chemical shifts of biologically relevant phosphates. Table reproduced from [1]

Adenosine monophoshate (AMP)		6.33
Adenosine diphosphate (ADP)	α	-7.05
	β	-3.09
Adenosine triphosphate	α	-7.52
	β	-16.26
	γ	-2.48
Dihydroxyacetone phosphate		7.56
Fructose-6-phosphate		6.64
Glucose-1-phosphate		5.15
Glucose-6-phosphate		7.20
Glycerol-1-phosphate		7.02
Glycerol-3-phosphorylcholine		2.76
Glycerol-3-phosphorylethanolamine		3.20
Inorganic phosphate		5.02
Phosphocreatine		0.00
Phosphoenolpyruvate		2.06
Phosphorylcholine		5.88
Phosphorylethanolamine		6.78
Nicotinamide adenine dinucleotide (NADH)		-8.30

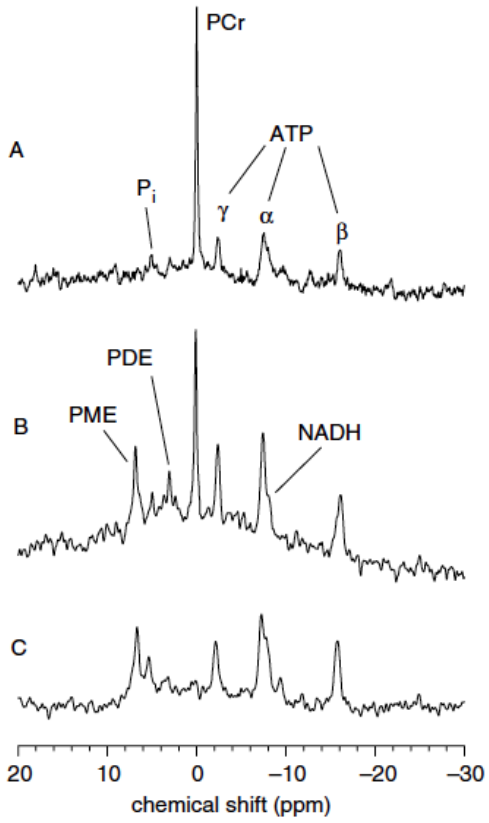

Figure 3.6: ^{31}P MRS spectra of different rat tissues in vivo. (A) muscle (B) brain (C) liver Figure reproduced from [1]

.

3.2.2 pH Determination in Tissue

An important physiological parameter is the intracellular pH value, which is an indirect parameter of muscle activity. The correlation between pH and chemical shift dispersion is caused by bonds with ions e.g. magnesium, which change the chemical environment of the individual nuclei and therefore the resonance frequency. [1]

The pH can be derived by the Hendersen-Hasselbach relationship as shown in (3.5) where δ is the observed chemical shift of a certain compound A. δ_A and δ_{HA} are the chemical shifts of the unprotonated and protonated states of the compound and pK_A is a constant which represents the acid-base equilibrium of the specific metabolite. [1]

$$pH = pK_A + log\left(\frac{\delta - \delta_{HA}}{\delta_A - \delta}\right) \tag{3.5}$$

Inorganic phosphate relative to phosphocreatine is the most commonly used resonance in ^{31}P MRS. measurements mainly because it can be observed in almost every tissue and it is highly sensitive to pH changes. [1].

Figure 3.7 shows the calibration curve for the Pi-PCr system with pK=6.77, δ_A=5.7 ppm and δ_{HA}=3.23 ppm.

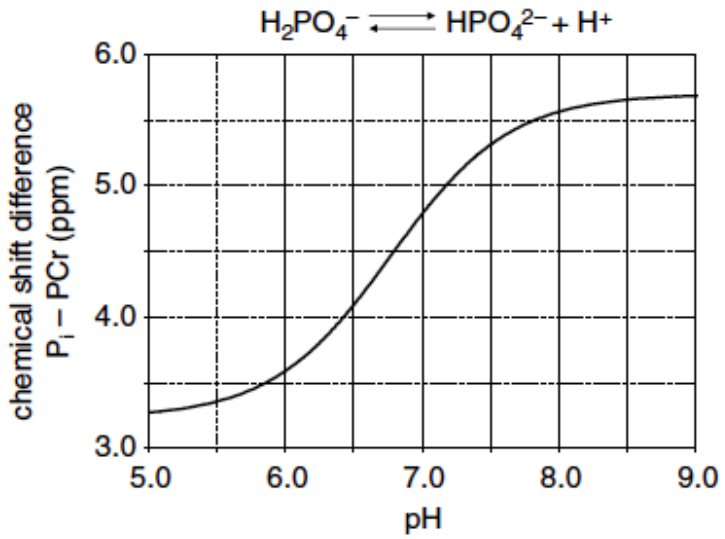

Figure 3.7: Chemical shift differences (ppm) as a function of pH value in phosphorus spectroscopy. Figure reproduced from [1]

3.3 Example: semiLASER

Localization by Adiabatic Selective Refocusing (LASER) is a sequence which uses adiabatic RF pulses for excitation and refocusing. SemiLASER uses conventional slice selective RF pulses for the excitation followed by adiabatic refocusing pulses to complete the localization of the 3D volume [11][8].

After one adiabatic full passage a position dependent phase and a non-linear B_1 field is caused by the frequency modulation and leads to signal extinction. A second AFP pulse refocuses the phase and reassembles the signal. Therefore a pair of adiabatic full passage pulses, which equals a 360 ° flip angle is used for refocusing the magnetization during a slice selective gradient is switched on and off as shown in Figure 3.8 [1].

As mentioned earlier in 2.6 surface coils are often used when high sensitivity is required but the main disadvantage is the highly inhomogeneous B_1 field especially in deeper lying areas [1], [14]. In case of ^{31}P MRS with a lower sensitivity compared to ^{1}H MRS the use of surface coils would be beneficial but conventional pulses linearly depend on B_1 amplitude resulting in an inhomogeneous nutation angle [14]. Adiabatic pulses are more insensitive to B_1 inhomogeneities and therefore allows to use surface coils.[1], [14]. The use of surface coils counteracts the loss in sensitivity due to localization which is essential when using ^{31}P MRS [1], [14].

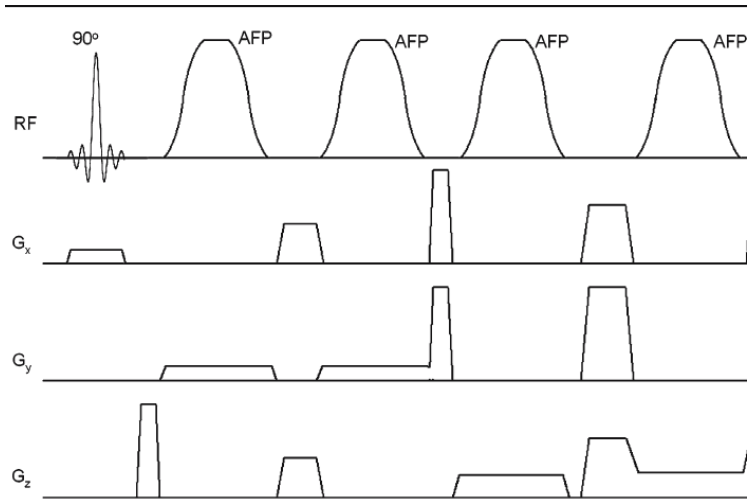

Figure 3.8: Excitation with a conventional slice selective RF-Pulse followed by 2 pair of adiabatic 180 degree (AFP) refocussing pulses reproduced from [11]

4 Methods

4.1 Introduction

A focus of the work of the MR group of the Center for Medical Physics and Biomedical Engineering at Medical University Vienna is ^{31}P MRS. Several research articles were published on the investigation of the metabolic response of different muscles tissues during physical exercise in a calf muscle in vivo [8], [9], [15]–[19].

A semi-LASER single voxel spectroscopy sequence [11] is used on a Siemens Magnetom 7T scanner for measurement on subjects. An originally CSI sequence was reprogrammed for SVS using IDEA (Integrated Development Environment for Applications) provided by Siemens to create the specific semi-LASER sequence with adiabatic refocusing pulses.

A typical measurement starts with the selection of a volume of interest (VOI) in a specific muscle tissue (Gastrocnemius, Soleus) [8]. During the measurement first the subject is instructed to perform physical exercise on a custom built ergometer, followed by a recovery time. At onset of exercise the phosphocreatine in the muscle tissue starts to decrease in concentration during exercise and accordingly the inorganic phosphate concentration starts to increase. During the recovery phase, the phosphocreatine starts to rise again in concentration while the inorganic phosphate slowly reaches its minimum.

To measure the dynamics of phosphorylated metabolites in a different muscle the whole procedure has to be repeated with a second volume of interest [9].

The goal of this master thesis was to extend the existing sequence to establish a multi voxel spectroscopy method where several VOI positions can be

selected and successively measured in a continuous train, yielding time-resolved ^{31}P spectra from several distinct regions in a muscle or in different muscles in an exercising limb [8], [9], [15], [17]–[19].

The advantage would be, that ideally the subject has to perform the exercise only once during the whole procedure and the signal of both muscle positions would be acquired.

A potential disadvantage is that if the voxels share one or more planes, the gradient direction during the excitation pulse should be normal to one of the free planes to avoid mutual interference. To ensure that the orientation parameter has to be set up correctly. Ideally the refocusing pulses should not affect the magnetization of the second voxel. Additionally the time resolution decreases to 50 % compared to Single Voxel Spectroscopy if during the same exercise duration two voxel of interests are measured instead of one.

After the data was acquired it was quantified with the jMRUI software package and the AMARES (Advanced Method Accurate Robust and Efficient Spectral Fitting) algorithm. The MR spectra shown in this thesis were generated by an already available python script which perform phasing and combining of the phosphor channels after line broadening and zero filling. The spectra were weighted to the amplitude peak.

4.2 Implementation of the Multi Voxel Acquisition Functions into the semi-LASER Sequence

SIEMENS provides a developing environment for MR sequence programing in C++ programming language for their customers with a research cooperation agreement. It is an environment with special functions to directly access almost every MR parameter in a sequence. In a specific sub function (RunKernel) the timing of the pulses and gradients can be precisely programed. There is also a specific unit test available to check if the sequence

satisfies all necessary requirements to check if it would run on the real MR scanner.

The ”Protocol offline editing tool” (POET) allows to run the sequence with the same interface as on the real scanner, as shown in Figure 4.1. While editing the parameters on the user interface the preparation function runs repeatedly in the background to check if the current settings are valid as on the real scanner. The simulation software pretends a measurement with the current data and visualizes it on a time-graph as shown in Figure 4.2. The different pulses and gradients are changing depending on the input parameters.

POET cannot test the image reconstruction which is done by the ”image calculation environment” (ICE) program. The ICE runs on a separate computer at the scanner.

The sequence code needs to pass the required information about the order of acquisitions to the ICE program correctly, to ensure correct reconstruction.

Spectroscopy sequences provided by Siemens are not used to allow multiple slice positions (slice groups) as, for example imaging sequences do and therefore the slice group parameter is not present in the user interface as shown in Figure 4.3. Siemens prevents programers to modify the standard user interfaces but allows access to the internal parameters via a programable special card which is originally empty.

To allow multiple voxel measurement in one MR sequence the slice group access had to be programed manually and therefore a loop structure was created which uses the already existing slice group array which contains the desired voxel positions accessed via the special card.

With the developed multi voxel sequence, the user can select the desired voxel position on the localizer and save the current voxel position by clicking on the apply button on the special card, as shown in Figure 4.4. The user is able to change the duration of the excitation and the adiabatic refocusing pulse for each voxel individually. This is important because in case one voxel is further away of the coil, it could be necessary to adapt the pulse voltages to ensure a 90° flip angle and a full 180° refocusing and this is limited by the SAR. To avoid that the pulse duration could be elongated for

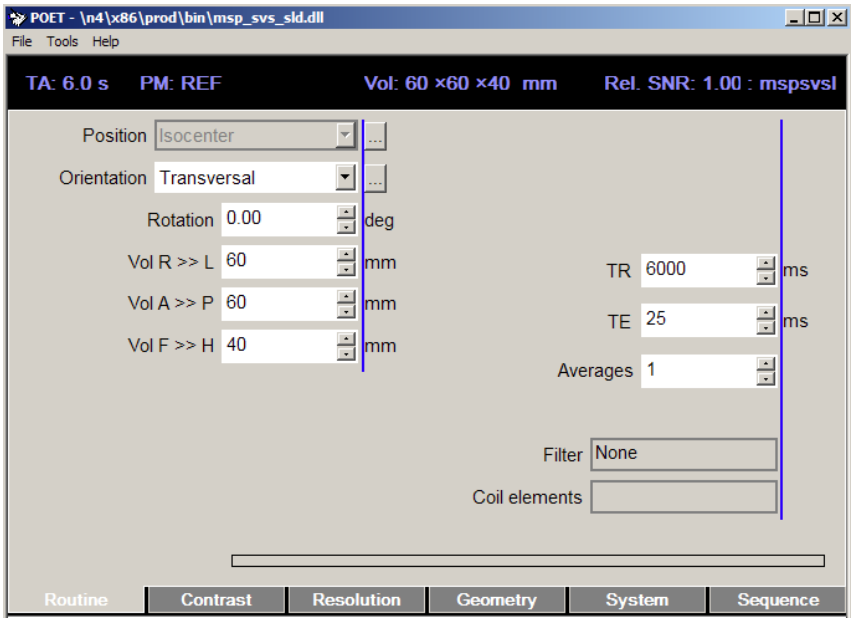

Figure 4.1: Protocol offline editing tool (POET) user interface

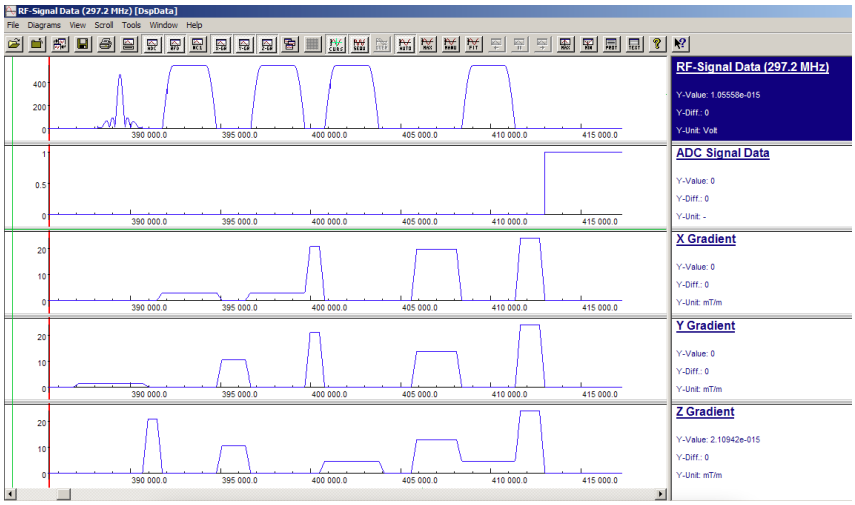

Figure 4.2: Sequence visualization with the POET Simulator.

each voxel individually and the delivered energy decreases so that the SAR limits will not be exceeded.

The reason why it is important to use the implemented slice group array instead of using custom variables or arrays is that the Siemens standard functions to access and pass the voxel data to other functions can still be used.

4.3 Measurement Setup Components for Testing the Functionality of the Multi Volume Acquisition

4.3.1 Phantom Composition with Different Compartments

To test the sequence on the 7T Scanner (Siemens AG Healthcare, Erlangen, Germany) in vitro measurements were applied and therefore a specific phantom was built. A transparent plastic cylinder 2.8 l was filled with potassium hydrogen phosphate solution at about 50 mMol/l concentration and added 1 ml/l Magnevist (Gadolinium) to increase T1 relaxivity. Inside the cylinder two 40 mm^3 voxels were placed and also filled with potassium hydrogen phosphate with the same concentration but different pH. Originally the pH of the potassium hydrogen phosphate solution was about 5.3.

The pH of the solution in the first voxel was about pH 5.3 and in the second voxel solution the pH was manipulated to about pH 7.5. The pH of the surrounding solution was changed to approximately 6.5. The pH manipulation was accomplished with NaOH pellets and carefully measured with an electronic pH-meter.

The voxels were placed side by side with approximately parallel side walls at the same depth inside the container. Shown in Figure 4.5 the left voxel position is later considered as position 1 and the right as position 2. These two voxel positions share 2 planes which is useful to test during multi voxel spectroscopy how the RF pulses of the first voxel affect the magnetization of the second.

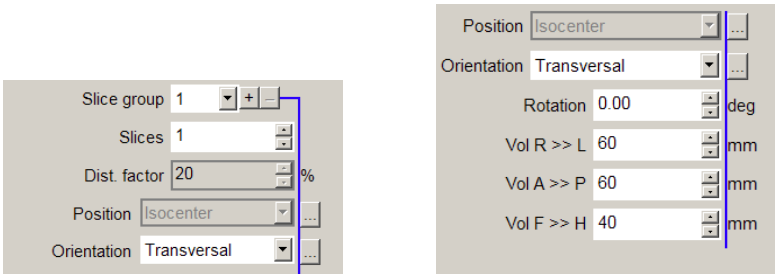

(a) Imaging Sequence (FLASH) (b) Spectroscopy Sequence

Figure 4.3: Comparison between the contrast cards of the standard user interface of an imaging sequence and a spectroscopy sequence. The slice group access is not available with spectroscopy sequences.

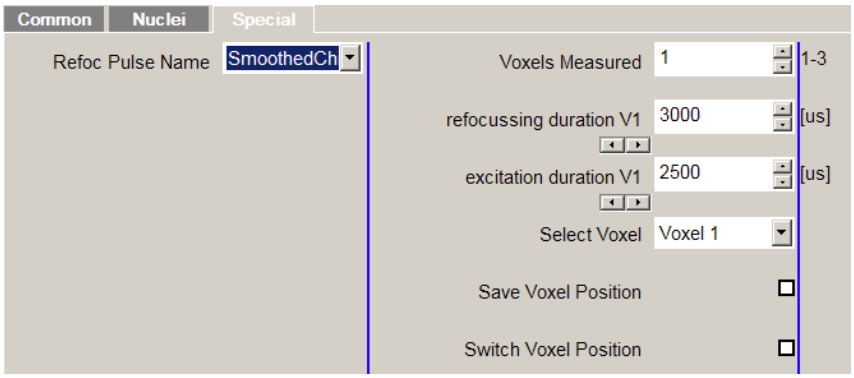

Figure 4.4: Customized special card in the multi voxel sequence

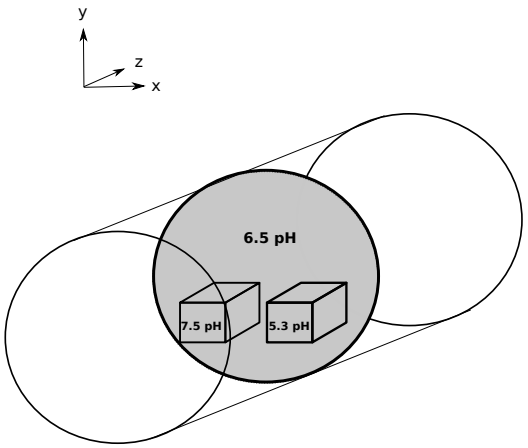

Figure 4.5: Phantom placement inside the scanner. The phosphor solution with pH 7.5 is placed at voxel position 1 and with pH 5.3 at voxel position 2.

4.3.2 Description of the Multichannel Transceiver RF-Coil Used for the Measurements

The coil used in this work was developed by the group of ZMPBMT/MUW in the RF lab. This coil is described in the publication of Goluch et al. 2014 [16] and the content of the following chapter mainly orientates on this publication.

For the phantom measurements in this thesis a form fitted ^{31}P ^{1}H multichannel transceiver coil array was used consisting of 5 channels (3 phosphorus 2 hydrogen) as shown in Figure 4.6. This coil array was specifically developed for studies of exercising human calf muscles at 7T [16]. 2 ^{1}H channels are enough to cover the calf muscle with a satisfactory homogeneity and were only used for the localizer image and the passive shim.

A number of three Phosphor channels were chosen because it is a good balance between increasing sensitivity and keeping the array design difficulties concerning decoupling acceptable low. [16]

When analyzing the energy metabolism with ^{31}P MRS there is always a

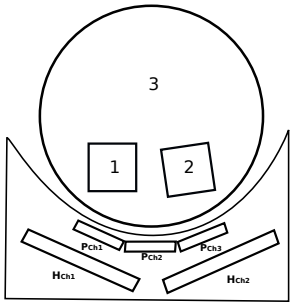

Figure 4.6: Schematic representation of the phantom and the tranceiver coil with three phosphorus and two hydrogen channels. Voxel 1, 2 and 3 representing the solutions with varying pH.

tradeoff between signal to noise ratio and temporal resolution or spatial localization. Localization improves the specificity of different metabolites and muscle tissues compared to non-localized methods but at the same time it decreases SNR. Keeping the SNR acceptable when using localization sequences can be achieved by improving the coil sensitivity [16].

If high sensitivity is desired surface coils are often used. Unfortunately these coils produce a highly inhomogeneous B_1^+ field and the sensitivity decreases dramatically while moving away from the coil. Birdcage type volume coils produce a B_1^+ field with higher homogeneity but lack of sensitivity compared to surface coils [16].

Using a phased array of surface coils combines the advantages of both surface and volume coils. To further increase the sensitivity the array coil should be form-fitted to the targeted anatomical form. The difficulty while working with phased arrays is the coupling between the individual array elements. To achieve decoupling there are several capacitive or inductive methods available [16].

In case of the 7T Magnetom scanner there is no body coil available which means the RF-coil needs to transmit and receive which is either done by separate transmit and receiver coils or using a combined transceiver coil with a built-in transmit/receive switch [16].

4.4 Transmit Voltage Adjustments for Flip Angle Optimization

After the phantom cylinder was fixed on the transceiver coil and was placed inside the magnet as shown in Figure 4.6, the localizer image was acquired with the two ^{1}H elements to place the shim adjust volume correctly and to set up the VOI as shown in Figure 4.7. A 37 mm^3 VOI was placed in one of the two 37 mm^{3}cubes inside the cylinder. Shimming was done with the ^{1}H channels. The reference voltage is defined as the value where a 0.5 ms square pulse excites the VOI with a 90 ° flip angle.

To ensure a 90 ° flip angle in the VOI, several measurements with $T_E = 40$ ms and increasing reference voltage between 50 V – 300 V were applied with the phosphor channels, to find the signal with the maximum amplitude and the corresponding reference voltage. Due to construction limits of the coil the voltages for each pulse were not allowed to exceed 250 V. The pulse voltages are calculated depending on the pulse shape and the reference voltage value. This had to be checked on the Transmitter/Receiver card shown in Figure 4.8a. If the voltages for the pulses went too high, the duration of the excitation pulse and the refocusing pulses had to be adjusted to allow further increase of the reference voltage and find the maximum signal peak Figure 4.8b.

If the duration of the pulses elongate it allows to deliver the same energy and generate the same flip angle with a lower amplitude (voltage). Unfortunately it increases also the echo time. The duration of the adiabatic refocusing pulse were set to 7.2 ms and the duration of the excitation pulse was set to 3.5 ms. The measurements were acquired for both voxel positions separately with single voxel spectroscopy.

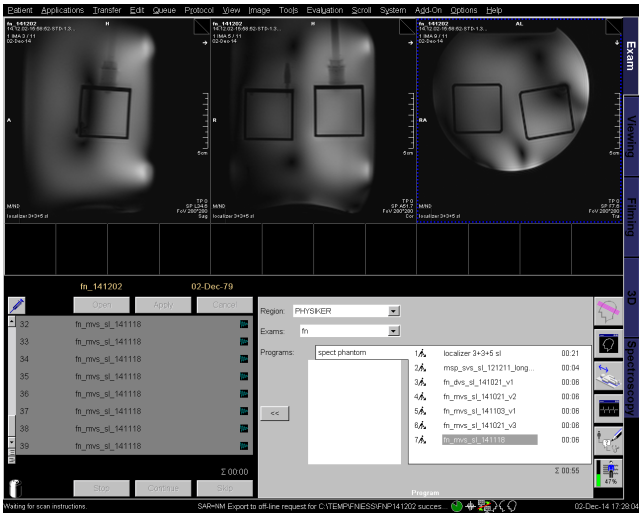

Figure 4.7: Localizer picture of the phantom on the Magnetom scanner acquired with a GRE - sequence.

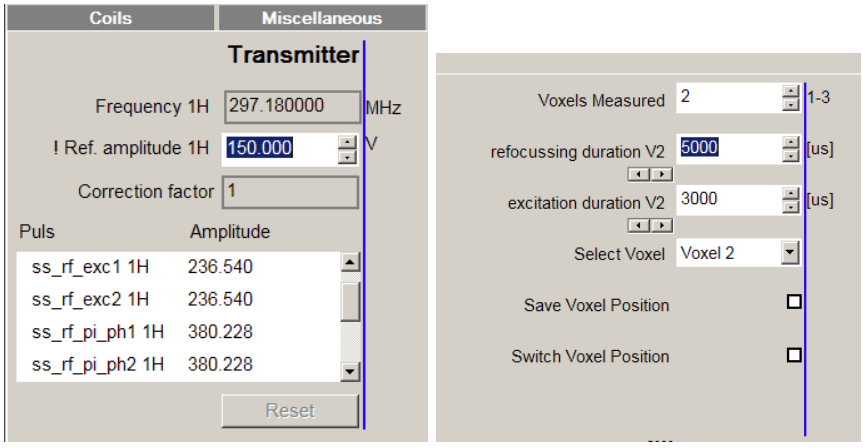

(a) (b)

Figure 4.8: (a) Transmitter voltage of the individual pulses should not exceed 250 V for safety reasons. (b) The duration of the excitation pulse and the refocusing pulses can be set individually for each voxel position

4.5 T1 Relaxation Time Determination of the Phantom Compartments

For analysis of the mutual saturation effects between voxel compartments when using a multi voxel acquisition technique, it is necessary to know the T1 relaxation times of each compartment in order to be able to calculate the evolution of the net magnetization over time after an ideal excitation. Measuring the T_1 relaxation time of each compartment was accomplished using a modified semiLASER sequence with an added inversion recovery pulse. The VOI was placed so, that it contained all three compartments of the phantom. The maximum signal amplitude was measured at a reference voltage about 180 V and the signal was acquired with 2048 points at a 5000 Hz bandwidth. The pulse length of both the inversion pulse and the excitation pulse were 5 ms, the echo time $T_E = 35$ ms and the T_R was set to 20 s. With 4 averages the inversion time T_I was increased from 0.05 s in 10 steps until 15 s (0.05 s, 0.1 s, 0.5 s, 1 s, 2 s, 3 s, 5 s, 10 s, 15 s, 20 s) after each measurement. The last measurement was applied without an inversion pulse ($T_R = 20$ s). The acquired data were fitted and plotted with gnuplot.

4.6 Demonstration of Mutual Saturation Effects between Volumes During an Interleaved Multi Voxel Acquisition

The challenge when working with an interleaving multi voxel spectroscopy sequence is the appropriate choice of the setup parameters especially if the same time resolution is desired as with single voxel spectroscopy. The more acquisitions are applied in the same amount of time the sooner SAR limits will be reached.

In case both voxels share one orthogonal slice the applied excitation and refocusing pulses of one voxel affect the magnetization of the other and vice versa. This can cause mutual saturation especially with short repetition times [10]. The orientation parameter on the user interface while selecting

the voxel plays an important role because it defines which slice selective gradient is switched on and off during the pulses.

In the phantom voxel 1 and voxel 2 both share the z plane and the y plane as shown in Figure 4.5. A gradient in z or y direction in combination with a RF pulse of a defined bandwidth selects the slice of the whole orthogonal direction and affects the magnetization of both voxel. Table 4.1 shows which gradient is switched on and off under each pulse with a transversal, sagittal or coronal orientation parameter. Obviously both coronal and sagittal orientation setups switch the z gradient on and off during the excitation pulse which directly affects the magnetization of both voxels and would cause saturation. With the transversal orientation only the refocusing pulses could affect the magnetization which is ideally negligible if perfect refocusing is assumed.

Table 4.1: Applied gradient directions during RF pulses in the semiLASER sequence by Scheenen et. al.[11]

Orientation	Exc. pulse	adiab. refoc. pulse 1	adiab. refoc. pulse 2
Transversal	$-x$	$-y$	$-z$
Coronal	$+z$	$+x$	$-y$
Sagittal	$-z$	$-y$	$+x$

As shown in Figure 5.1 the 90 ° flip angle was located approximately at a reference voltage of 220 V which would not allow two acquisitions with an overall T_R under 9 s due to SAR limitations. A maximum T_R of 8 s was desired to keep the time resolution acceptable and since the curve at the maximum is relatively flat a reference voltage of 200 V was chosen for all further measurements.

To illustrate the influence of the orientation setup parameter, three MVS measurements were applied with 20 repetitions, varying the orientation between transversal, sagittal and coronal with a very short T_{R1} time after the first acquisition ($T_{R1} = 1000$ ms). The repetition time of the second aciquisition was $T_{R2} = 7000$ ms and this results in a total TR of 8 s for one dual voxel acquisition.

4.7 Dynamic localized ^{31}P-MRS of Exercising Human Gastrocnemius and Soleus Muscle In Vivo Acquired with Multi Volume Acquisition Technique

To demonstrate the usability of the multi voxel spectroscopy sequence, a dynamic measurement of an exercising human calf muscle in-vivo was performed on a volunteer. The exercise was accomplished with a custom built non magnetic ergometer which allows to increase the resistance of the exercising pedal [8], [9]. Signals of both muscles gastrocnemius and soleus were acquired with $T_R = 6\,s(3\,s + 3\,s)$ and a $T_E = 29\,ms$ for each acquisition. Figure 4.9 shows the localizer picture of the calf muscle and the voxel placement with the excitation slice marked in red. The orientation parameter for both voxel were set to transversal and the gastrocnemius voxel was rotated clockwise to avoid an overlap of the excitation slice with the soleus voxel. Both voxel also share the z and y plane but since only the refocusing pulses could cause mutual saturation it was neglected according to previous results. The measurement composites of 2 exercise bouts with 2 min rest, 3 min exercise and 4 min recovery for the first bout with 0.35 bar resistance-pressure and 3 min exercise, 7 min recovery for the second bout with 0.55 bar resistance-pressure.

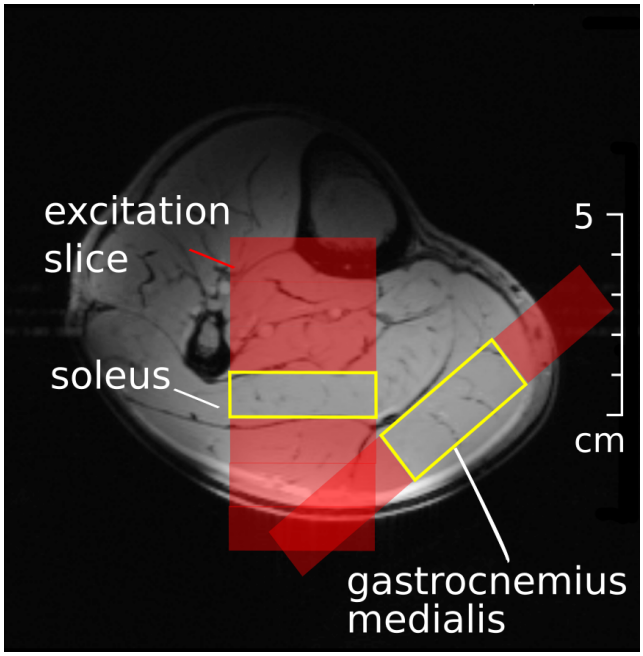

Figure 4.9: Localizer picture of the multi voxel spectrocopy setup in both gastrocnemius and soleus muscle. Both voxel orientation were set to transversal to avoid mutual interference in the z and y plane. The gastrocnemius voxel was rotated clockwise to avoid saturation of the soleus voxel due excitation of the gastrocnemius voxel.

5 Results

5.1 Maximum Signal Amplitude of the Voxel Compartments in the Phantom

As shown in Figure 5.1, the received signal peak increases with higher reference voltage until a 90° flip angle is reached. Further increasing of the reference voltage decreases the signal peak because the flip angle already passed 90° and the net magnetization after excitation is not fully in the transversal plane.

After finding the maximum amplitude for both voxel it was discovered that the signal amplitude of the voxel at position 2 was significantly lower compared to the voxel at position 1 even though both liquids had the same concentration (50 mMol/l). To ensure that the phantom was set up correctly, the two cube positions were switched mechanically and the measurement was repeated as shown in Figure 5.2. Fewer measurement points were acquired because the region of the maximum could be estimated from the previous measurement. The voxel at position 2 again showed a weaker signal amplitude compared to the voxel at position 1. The acquired signals for the same voxel positions in both measurements are comparable, as shown in Figure 5.3 and Table 5.1 which leads to the conclusion the B_1^+ field produced by the coil at voxel position 2 is lower than to the coil at voxel position 1. Due to the reciprocity principle, it is assumed that with a lower B_1^+ field a higher reference voltage is required to achieve a 90° flip angle, which is consistent with the results shown in Figure 5.1 and Figure 5.2. In Figure 5.1 the curve is relatively flat, which could be the reason that the maximum cannot clearly be determined.

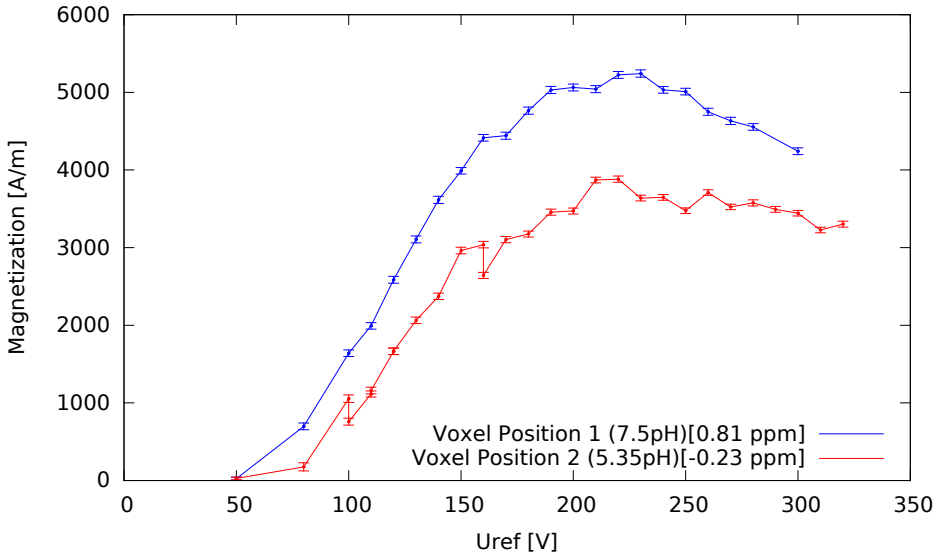

Figure 5.1: Signal amplitude vs. increasing reference voltage. The maximum signal peak approaches a 90° flip angle. Data was quantified and exported with jMRUI and AMARES and plotted with gnuplot.

Table 5.1: Single voxel spectroscopy spectra of voxel 1 and 2 with switched positions.

	Signal peak [a.u]	Noise peak [a.u]	SNR	FWHM [Hz]
pH 7.5 left	8.17e+05	4.19e+03	194.8	3.1
pH 5.3 left	9.65e+05	4.61e+03	209.3	2.7
pH 7.5 right	5.74e+05	3.83e+03	149.8	3.8
pH 5.3 right	5.40e+05	3.73e+03	144.7	3.5

5.1 Maximum Signal Amplitude of the Voxel Compartments in the Phantom

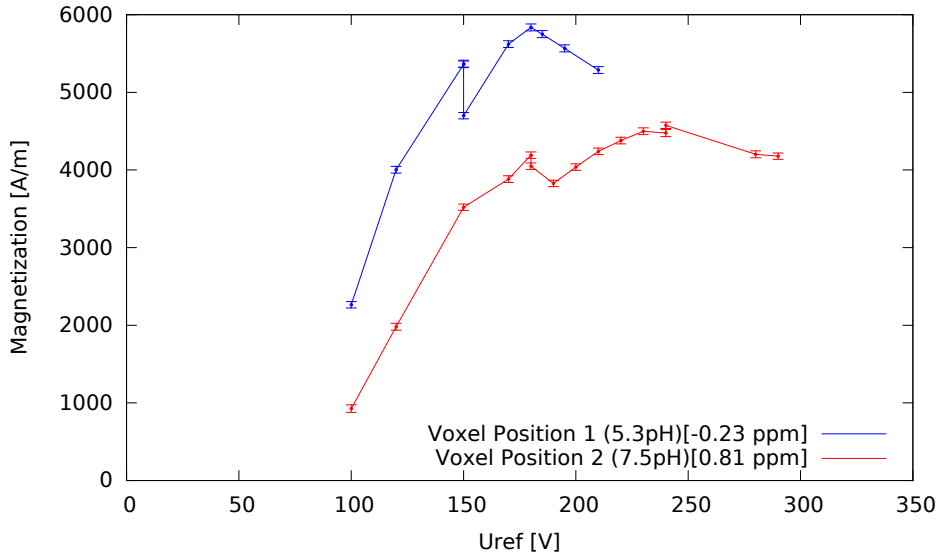

Figure 5.2: Signal ampltude vs. increasing reference voltage. The voxel positions are mechanically switched. The maximum signal peak approaches a 90° flip angle. Data was quantified and exported with jMRUI and AMARES and plotted with gnuplot.

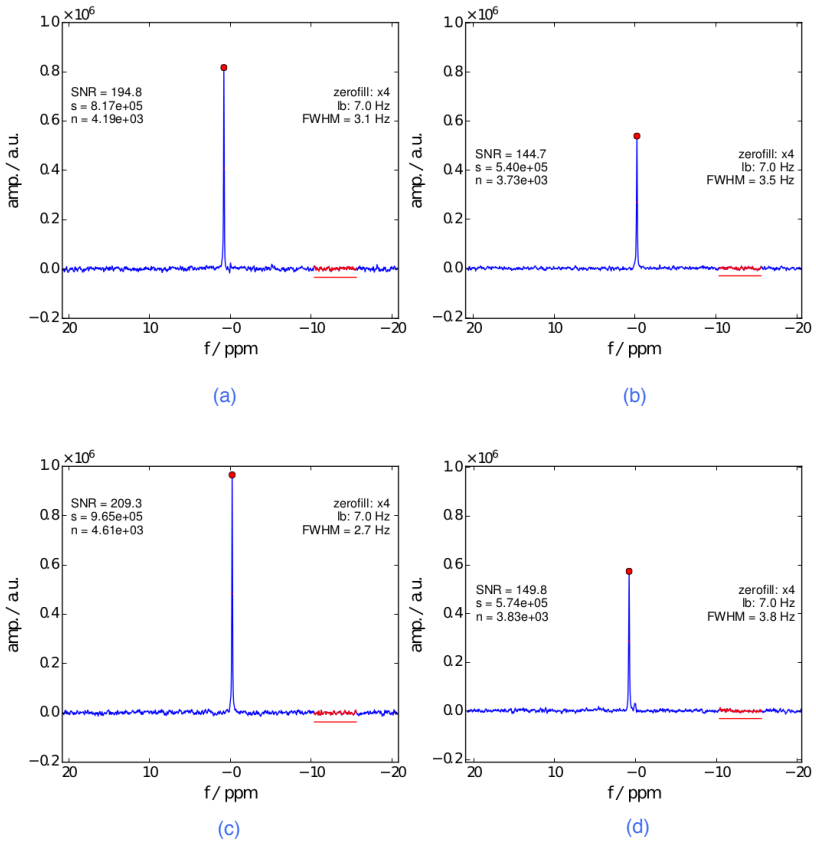

Figure 5.3: Spectrum of the weighted average of 3 Phosphor channels representing the maximum amplitude of (a) Voxel at position 1 with pH 7.5 (b) Voxel at position 2 with pH 5.3 (c) Voxel at position 1 with pH 5.3 (d) Voxel at position 2 with pH 7.5

5.2 T1 Relaxation Times of the Phantom Compartments

The trend of the magnetization over time is shown in Figure 5.4 and the resulting T_1 relaxation times fitted by gnuplot are shown in Table 5.2.

The differences of the signal amplitude between the three compartments which can be seen in Figure 5.4a occured because of the B_1^+ inhomogeneities of the transceiver coil and slight variations in size of the subcompartments. A normalized T_1 fit is shown in Figure 5.4b where the differences of the T1 time is more evident.

5.3 Comparison of Results between Single and Multi Voxel Spectroscopy

Mutual influence between volumes during an interleaved multi volume acquisition is not desired and should be prevented. Ideally the results acquired with both Single and Multi Voxel Spectroscopy technique should not differ.

Figure 5.5 shows the spectra of the left voxel with 7.5 pH one second after the acquisition of the right voxel with 5.3 pH with different orientation parameters. One single voxel spectroscopy spectra was measured separately with $T_R = 8\,s$ and also 20 repetitions as a reference. All spectra were averaged by the factor 5 during post processing.

Table 5.2: T_1 relaxation time given as fit results $\pm$ Standard Deviation as returned by the fit routine

	T_1 [s]	$\pm$ SD [s]
7.5 pH	4.05	0.09
6.5 pH	3.34	0.06
5.3 pH	3.02	0.11

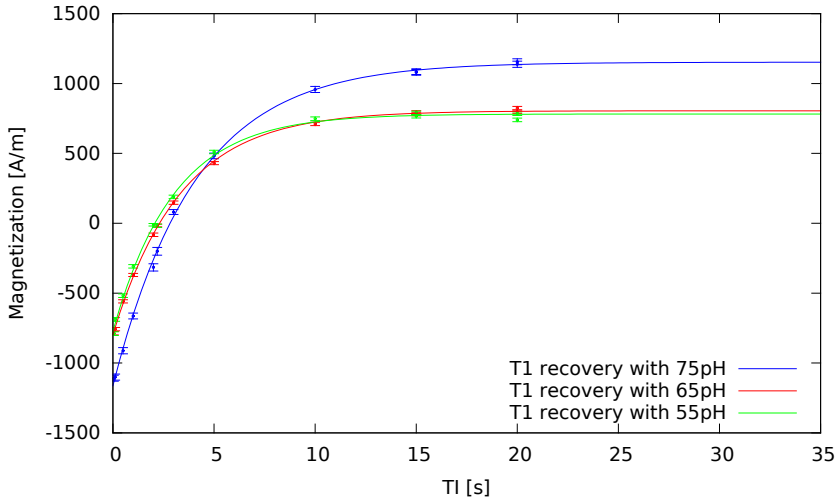

(a)

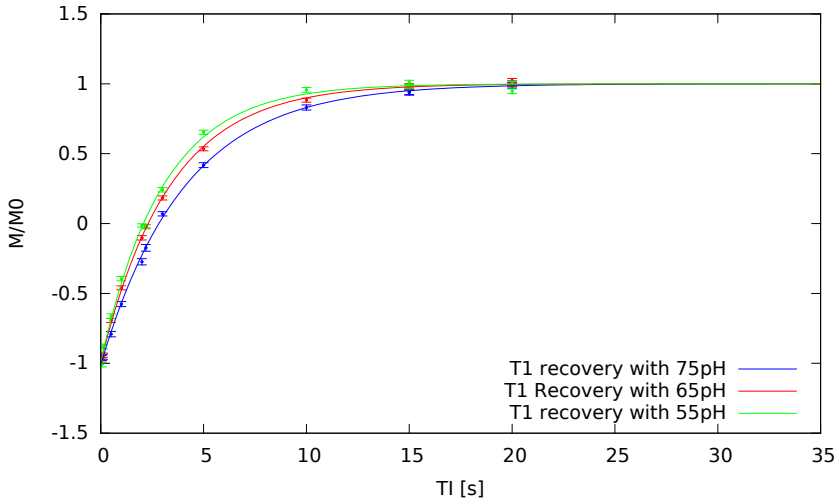

(b)

Figure 5.4: T_1 recovery curve of the three compartments with increasing inversion time with (a) absolute and (b) normalized values.

As shown in Figure 5.5 and Table 5.3 the amplitude of the left voxel with 7.5 pH clearly was influenced by the previous acquisition of the right voxel with 5.3 pH compared to the reference single voxel spectroscopy. With a sagittal or coronal orientation the signal amplitude decreases dramatically to about 35-40 % which was expected because according to Table 4.1 the excitation pulse of the first acquisition saturates the magnetization of the z slice. With a transversal orientation the amplitude of the signal decreases to about 86 % due to the influence of the refocusing pulses. This could be the reason of the lower reference voltage which results in slight deviation from a 180 ° flip angle during refocusing.

The measurement was repeated with both voxels in reverse order again with similar results as shown in Figure 5.6 and Table 5.4.

The values of TR_1 and TR_2 were changed to 4 seconds to demonstrate the benefit of the multi voxel spectroscopy, acquiring spectra of two voxels in the same time compared to a single voxel spectroscopy measurement without a noticeable loss of signal amplitude and SNR. For the MVS the orientations of both voxels were set to transversal to only let the refocusing pulses affect the shared slices of both voxels and the measurement was repeated in both constellations (right-left and left-right). The number of repetitions for all measurements was set to 10 and the results shown in Figure 5.8 were averaged ($N = 5$) with a python script to enhance the SNR. The very first acquisition was excluded.

The results shown in Table 5.5 and Figure 5.8 illustrate that even with an

Table 5.3: Multi voxel spectroscopy signals ($T_{R1} = 1000$ ms and $T_{R2} = 7000$ ms) of the second acquired voxel (left with pH 7.5) with different orientations (Transversal, Sagittal, Coronal) of the first voxel. compared to a single voxel spectroscopy (SVS) acquisition as reference.

	Signal peak [a.u]	Noise peak [a.u]	SNR	FWHM [Hz]
SVS	5.77e+05	2.47e+03	233.6	7.6
Transversal	4.97e+05	2.37e+03	209.9	7.4
Sagittal	2.11e+05	2.36e+03	89.4	8.3
Coronal	2.30e+05	1.99e+03	115.8	7.8

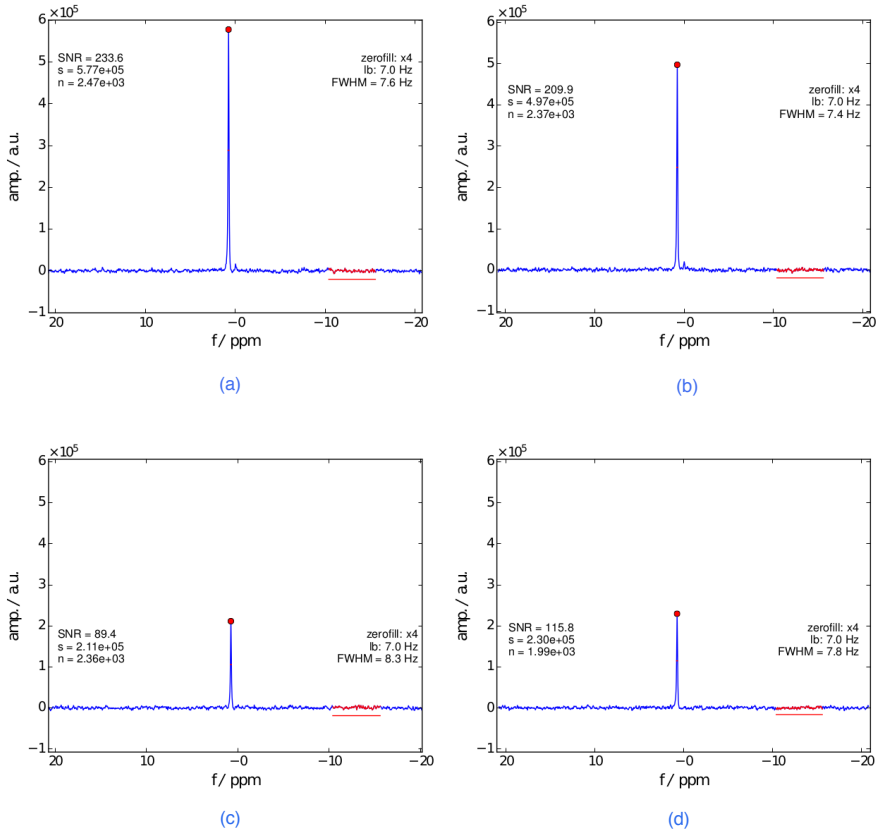

Figure 5.5: Spectra of the second acquired voxel with pH 7.5 at position 2 during multi voxel spectroscopy with $T_{R1} = 1000\,\text{ms}$ and $T_{R2} = 7000\,\text{ms}$. (a) single voxel spectroscopy (b) transversal orientation, (b) sagittal orientation (c) coronal orientation of the first excited voxel.

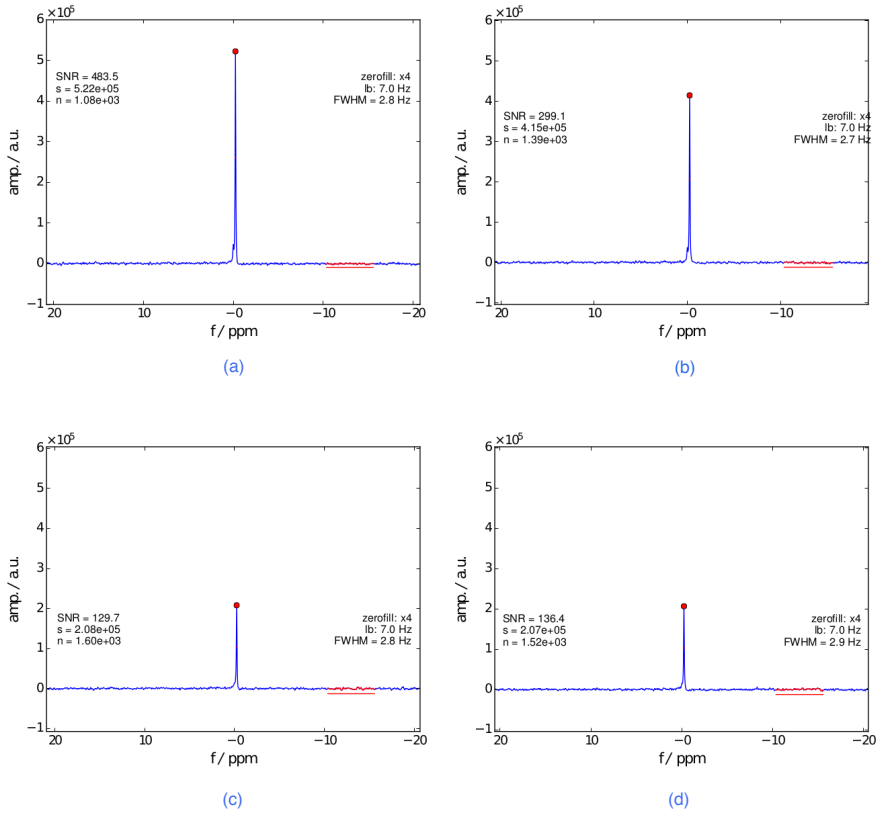

Figure 5.6: Spectra of the second acquired voxel with pH 5.3 at position 2 during multi voxel spectroscopy with $T_{R1} = 1000\,\text{ms}$ and $T_{R2} = 7000\,\text{ms}$. (a) single voxel spectroscopy (b) transversal orientation, (b) sagittal orientation (c) coronal orientation of the first excited voxel.

Table 5.4: Multi voxel spectroscopy signals ($T_{R1} = 1000\,\text{ms}$ and $T_{R2} = 7000\,\text{ms}$) of the second acquired voxel (right with pH 5.3) with different orientations (Transversal, Sagittal, Coronal) of the first voxel compared to a single voxel spectroscopy (SVS) acquisition as reference.

	Signal peak [a.u]	Noise peak [a.u]	SNR	FWHM [Hz]
SVS	5.22e+05	1.08e+03	483.5	2.8
Transversal	4.15e+05	1.39e+03	299.1	2.7
Sagittal	2.08e+05	1.60e+03	129.7	2.8
Coronal	2.07e+05	1.52e+03	136.4	2.9

imperfect refocusing flip angle $< 180°$ the signal amplitude and SNR of the multi voxel acquisition is about 95 % compared to single voxel acquisition with 10 repetitions. The loss in signal amplitude to about 86 % after one second due to influence of the refocusing pulses mentioned earlier compensates with a more reasonable choice of repetition time and in this specific case it relaxates back to 95 % according to (5.1) as shown in Figure 5.7.

$$M(t) = M_0(1 - e^{-T_R/T_1}) \tag{5.1}$$

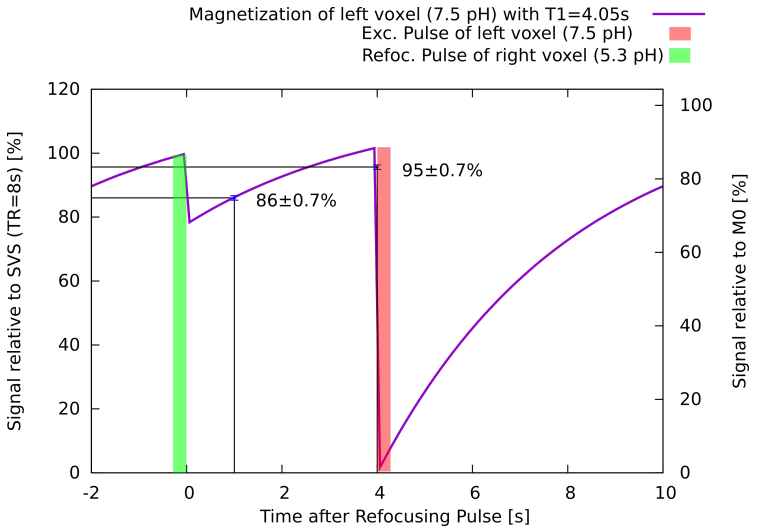

Figure 5.7: The Magnetization of the left voxel (7.5 pH) between two acquisitions ideally relaxates back to 100 % of SVS magnitude (TR=8 s). After the refocusing pulse of the right voxel (5.3 pH) the longitudinal magnetization is only 86 % refocused after 1 second as measured previously. With an repetition time of $T_{R1} = T_{R2} =$ 4 s between each voxel acquisition there is enough time for the longitudinal magnetization to relaxate back to about 95 %.

Table 5.5: Comparison between single and multi voxel spectroscopy spectra with a overall T_R=8 s(4 s+4 s). Measurements were applied in both constellations (right-left, left-right). 1st and 2nd means if the Voxel was measured first or second.

	Signal peak [a.u]	Noise peak [a.u]	SNR	FWHM [Hz]
pH 7.5 SVS	5.75e+05	2.68e+03	214.5	7.5
pH 7.5 MVS (1st)	5.48e+05	2.46e+03	222.6	7.4
pH 7.5 MVS (2nd)	5.50e+05	2.69e+03	204.2	7.6
pH 5.3 SVS	5.22e+05	1.08e+03	483.5	2.8
pH 5.3 MVS (1st)	4.87e+05	1.28e+03	381.7	2.7
pH 5.3 MVS (2nd)	4.85e+05	1.28e+03	379.4	2.7

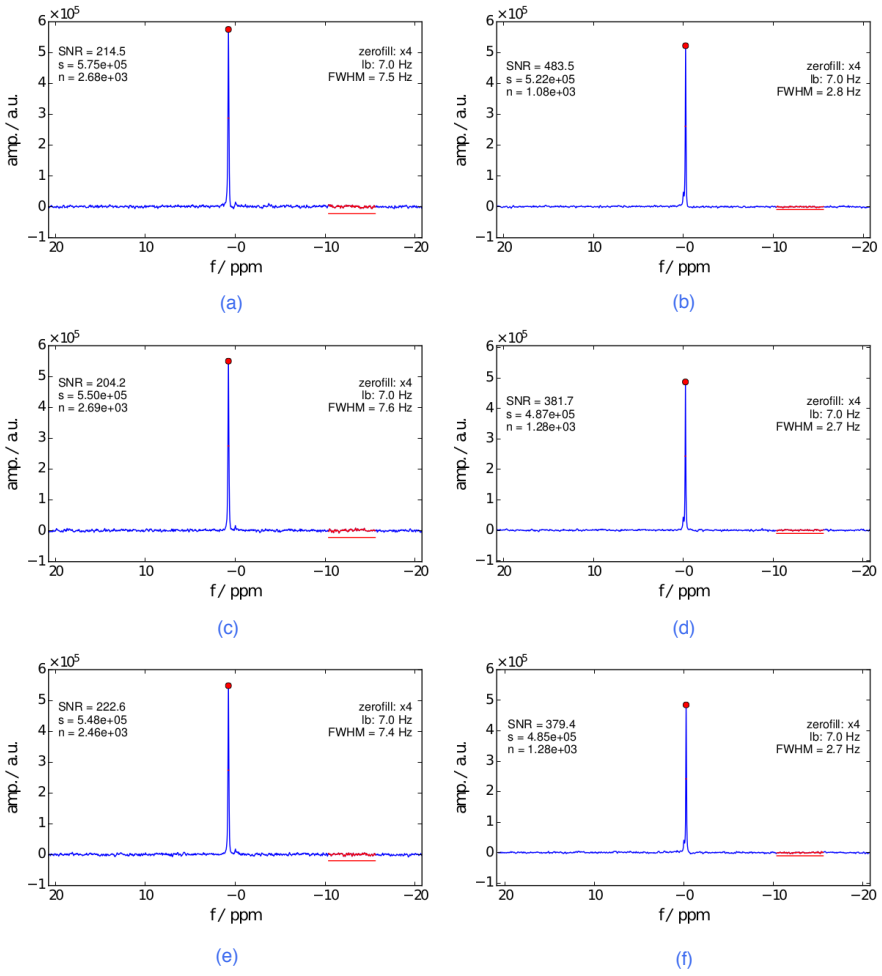

Figure 5.8: Spectra of 3 measurement setups with an effective TR of 8s (a) SVS of the left voxel with pH 7.5 (b) SVS of the right voxel with pH 5.3 (c) MVS of the left voxel (measured second) (d) MVS of the right voxel (measured first) (e) MVS of the left voxel (measured first) (f) MVS of the right voxel (measured second)

5.4 PCr Depletion and Recovery of Human Calf Muscles In Vivo

Figure 5.9 shows the phosphocreatine depletion and recovery with increasing time. Inorganic phosphate increases its concentration during exercise and slightly shifts the frequency due to protonation of the compound corresponding to Figure 3.7. The acquired rawdata of the 3 phosphor channels were phased and combined during postprocessing and the stackplot was created with a python script. The data was quantified with AMARES / jMRUI exported into a textfile and plotted via gnuplot for each bout seperately as illustrated in Figure 5.10 and Figure 5.11. To calculate the PCr Recovery time constant τ_{Recovery} an monoexponential curve was fitted in the recovery data and the results are shown in Table 5.6 and Table 5.7.

Table 5.6: PCr recovery fit constants of both muscles and bouts of the first measurement

Muscle and Bout	τ_{Recovery}[s]	$\pm$ SD[s]
Gastrocnemius Bout 1	274.62	79.44
Gastrocnemius Bout 2	90.96	4.18
Soleus Bout 1	36.42	7.32
Soleus Bout 2	34.32	2.88

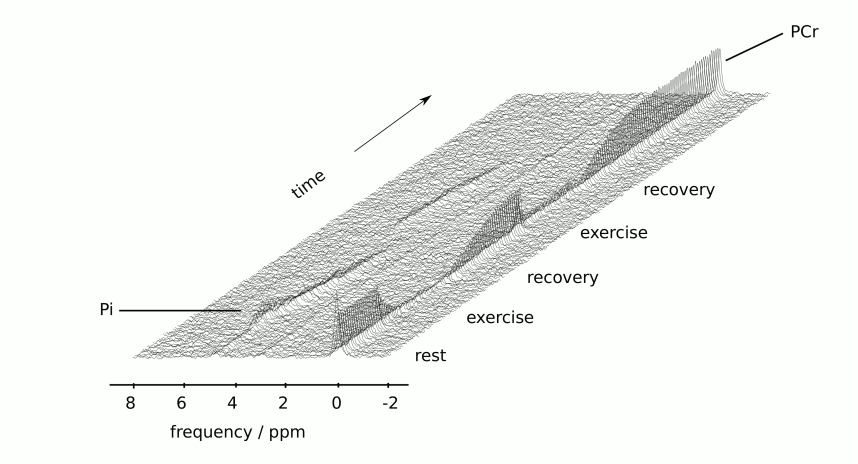

(a)

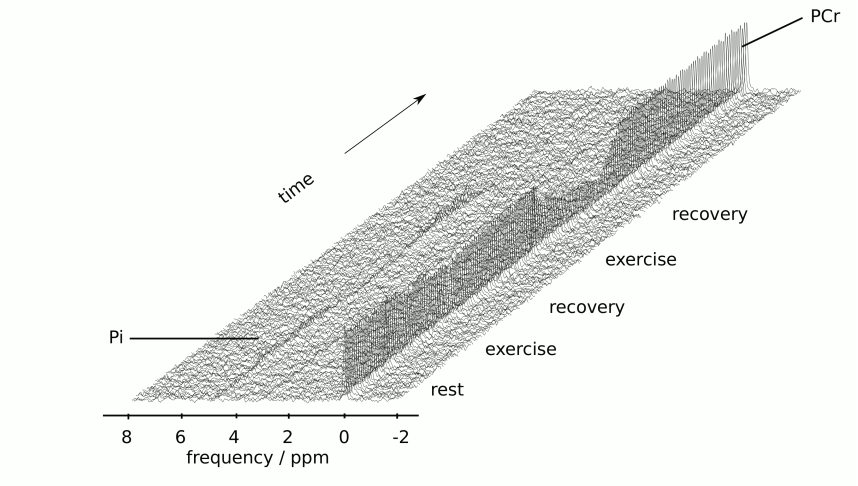

(b)

Figure 5.9: Stack plots of ^{31}P spectra acquired with the dual voxel spectroscopy sequence (semi-LASER) of an exercising human calf muscle in (a) musculus gastrocnemius (GM) (b) musculus soleus (SOL). Two different bouts were performed with increasing intensity (higher resistance in the ergometer)

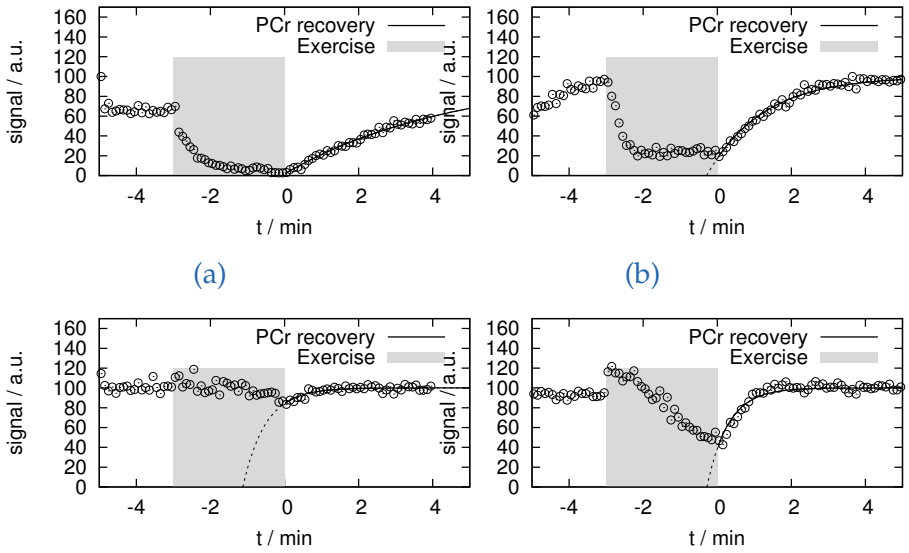

Figure 5.10: PCr recovery fits of two bouts with different resistance pressure on the ergometer pedal in musculus gastrocnemius (a) bout 1 with 0.35 bar (b) bout 2 with 0.55 bar and musculus soleus (a) bout 1 with 0.35 bar and (b) bout 2 with 0.55 bar.

Table 5.7: PCr recovery fit constants of both muscles and bouts of the second measurement

Muscle and Bout	τ_{Recovery}[s]	$\pm$ SD[s]
Gastrocnemius Bout 1	70.92	5.82
Gastrocnemius Bout 2	75.00	3.96
Soleus Bout 1	68.16	34.08
Soleus Bout 2	31.38	2.82

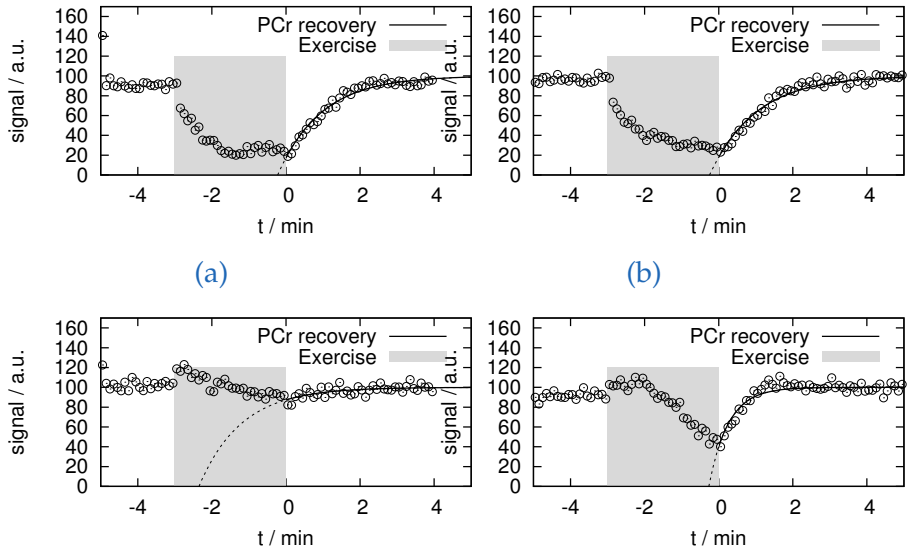

Figure 5.11: PCr Recovery fits of the second repetition of the multi voxel measurement with the same measurement setup. (a) Gastrocnemius bout 1 with 0.35 bar resistence-pressure (b) Gastrocnemius bout 2 with 0.55 bar (c) Soleus bout 1 with 0.35 bar and (d) Soleus bout 2 with 0.55 bar

6 Discussion

The principle of acquiring two spectra of two different voxel positions with an interleaving approach was already established 1991 by Ernst and Henning [10] but while their approach completely avoids an overlap of any orthogonal slice of both voxel during localization by tilting the gradients, this thesis presents a method where two orthogonal slices are shared while refocusing pulses are applied.

The results shown in 5.3 illustrate that with the Multi voxel spectroscopy semiLASER sequence two interleaving acquisitions of two different volumes within a repetition time of $T_R = 8\,s(4\,s + 4\,s)$ is comparable to results of the same volumes acquired separately with the same repetition time for each measurement. The signal amplitude and SNR of the multi voxel and single voxel approach corresponds to over 95 % although the refocusing pulses were not ideal and affect both voxel simultaneously during localization of each voxel. With a slight deviation from 180 ° refocusing due to a lower reference voltage, which was the case in that specific measurements, the signal amplitude decreased to about 86 % shortly after the refocusing pulses but recovered to about 95 % after 4 s due to relaxation as shown in Figure 5.7.

With the ideal reference voltage the SAR limits would have forced the T_R to elongate over 9 s and therefore the lower reference voltage was chosen to allow an T_R of 8 s.

By choosing a 10 % lower reference voltage, the slightly lower signal amplitude (93 % of the maximum, acquired with a single acquisition, shown in Figure 5.1) was accepted in favor of a higher time resolution which is important in case of dynamic measurements. It is expected that with the ideal reference voltage the difference between the results of the multi voxel acquisition and the single voxel acquisition would be negligible.

In section 5.4 the practical application of the multi voxel acquisition is shown during a dynamic ^{31}P MRS measurement of exercising calf muscles (Gastrocnemius and Soleus).

The resulting recovery time constants of the soleus muscle in the first exercise bout shown in table 5.6 and 5.7 were difficult to fit because a high depletion of the soleus at a low intensity is not always present. The analysis of the metabolic response of different muscle tissues is beyond the scope of this master thesis but will be discussed in the work of Fiedler. et al. [15].

Appendix

Bibliography

[1] R. A. de Graaf, *In Vivo NMR Spectroscopy*, L. John Wiley Sons, Ed., 978-0-470-02670-0. Wiley, 2007, vol. Second Edition (cit. on pp. 1, 2, 5–8, 12–15, 19–33).

[2] E. M. Purcell, H. C. Torrey, and R. V. Pound, "Resonance absorption by nuclear magnetic moments in a solid," *Physical Review*, vol. 69, no. 127, 1946 (cit. on p. 1).

[3] F. Bloch, W. W. Hansen, and M. Packard, "Nuclear induction," *Physical Review*, vol. 69, no. 127, 1946 (cit. on p. 1).

[4] W. G. Proctor and F. C. Yu, "The dependence of a nuclear magnetic resonance frequency upon chemical compound.," *Physical Review*, vol. 77, no. 717, 1950 (cit. on p. 1).

[5] W. Dickinson, "Dependence of the f19 nuclear resonance position on chemical compound.," *Physical Review*, vol. 77, no. 736, 1950 (cit. on p. 1).

[6] R. R. Ernst and W. A. Anderson, "Application of fourier transform spectroscopy to magnetic resonance," *Review of Scientific Instruments*, vol. 37, no. 1, pp. 93–102, 1966. DOI: http://dx.doi.org/10.1063/1.1719961 (cit. on p. 2).

[7] R. B. Moon and J. H. Richards, "Determination of intracellular ph by 31p magnetic resonance.," *Journal of Biological Chemistry*, vol. 248, no. 7276-7278, 1973 (cit. on p. 2).

[8] M. Meyerspeer, T. Scheenen, A. I. Schmid, T. Mandl, E. Unger, and E. Moser, "Semi-laser localized dynamic 31p magnetic resonance spectroscopy in exercising muscle at ultra-high magnetic field," *Magnetic Resonance in Medicine*, vol. 65, no. 5, pp. 1207–1215, 2011, ISSN: 1522-2594. DOI: 10.1002/mrm.22730 (cit. on pp. 2, 3, 24, 28, 33, 35, 36, 47).

[9] M. Meyerspeer, S. Robinson, C. I. Nabuurs, T. Scheenen, A. Schoisengeier, E. Unger, G. J. Kemp, and E. Moser, "Comparing localized and nonlocalized dynamic 31p magnetic resonance spectroscopy in exercising muscle at 7t," *Magnetic Resonance in Medicine*, vol. 68, no. 6, pp. 1713–1723, 2012, ISSN: 1522-2594. DOI: 10.1002/mrm.24205 (cit. on pp. 2, 3, 20, 25, 35, 36, 47).

[10] T. Ernst and J. Hennig, "Double-volume 1h spectroscopy with interleaved acquisitions using tilted gradients," *Magnetic Resonance in Medicine*, vol. 20, no. 1, pp. 27–35, 1991, ISSN: 1522-2594. DOI: 10.1002/mrm.1910200104 (cit. on pp. 3, 45, 65).

[11] T. W. J. Scheenen, A. Heerschap, and D. Klomp, "Towards 1h-mrsi of the human brain at 7t with slice-selective adiabatic refocusing pulses," English, *Magnetic Resonance Materials in Physics, Biology and Medicine*, vol. 21, no. 1-2, pp. 95–101, 2008, ISSN: 0968-5243. DOI: 10.1007/s10334-007-0094-y (cit. on pp. 3, 33–35, 46).

[12] R. Stollberger, *Bioimaging*, 2014 (cit. on pp. 5, 7–11, 14).

[13] M. A. Brown and R. C. Semelka, *MRI: Basic Principles and Applications, 4th Edition*. Wiley-Blackwell, 2010, vol. Fourth Edition (cit. on p. 14).

[14] A. Tannus and M. Garwood, "Adiabatic pulses," *NMR In Biomedicine*, vol. 10, no. 423-434, 1997 (cit. on pp. 15–17, 33).

[15] G. B. Fiedler, M. Meyerspeer, A. I. Schmid, S. Goluch, K. Schewzow, E. Laistler, A. Mirzahosseini, F. Niess, E. Unger, M. Wolzt, and E. Moser, "Localized semi-laser dynamic 31 p magnetic resonance spectroscopy of the soleus during and following exercise at 7 t," *Magnetic Resonance Materials in Physics Biology and Medicine*, 2015. DOI: 10.1007/s10334-015-0484-5 (cit. on pp. 35, 36, 66).

[16] S. Goluch, A. Kuehne, M. Meyerspeer, R. Kriegl, A. I. Schmid, G. B. Fiedler, T. Herrmann, J. Mallow, S.-M. Hong, Z.-H. Cho, J. Bernarding, E. Moser, and E. Laistler, "A form-fitted three channel 31p, two channel 1h transceiver coil array for calf muscle studies at 7 t," *Magnetic Resonance in Medicine*, n/a–n/a, 2014, ISSN: 1522-2594. DOI: 10.1002/mrm.25339 (cit. on pp. 35, 41, 42).

[17] K. Schewzow, M. Andreas, E. Moser, M. Wolzt, and A. I. Schmid, "Automatic model-based analysis of skeletal muscle bold-mri in reactive hyperemia," *Journal of Magnetic Resonance Imaging*, vol. 38, no. 4, pp. 963–969, 2013, ISSN: 1522-2586. DOI: 10.1002/jmri.23919 (cit. on pp. 35, 36).

[18] K. Schewzow, G. B. Fiedler, M. Meyerspeer, S. Goluch, E. Laistler, M. Wolzt, E. Moser, and A. I. Schmid, "Dynamic asl and t2*-weighted mri in exercising calf muscle at 7 t: a feasibility study," *Magnetic Resonance in Medicine*, n/a–n/a, 2014, ISSN: 1522-2594. DOI: 10.1002/mrm.25242 (cit. on pp. 35, 36).

[19] A. I. Schmid, K. Schewzow, G. B. Fiedler, S. Goluch, E. Laistler, M. Wolzt, E. Moser, and M. Meyerspeer, "Exercising calf muscle t2* changes correlate with ph, pcr recovery and maximum oxidative phosphorylation," *NMR in Biomedicine*, vol. 27, no. 5, pp. 553–560, 2014, ISSN: 1099-1492. DOI: 10.1002/nbm.3092 (cit. on pp. 35, 36).